https://doi.org/10.5194/egusphere-2026-6810
Preprint. Discussion started: 25 November 2026
© Author(s) 2026. CC BY 4.0 License.

Contrasting large river basins are characterized by high fractions of young water and show differences in water-age dynamics across flow conditions and seasons

Karl Knaebel[1], Markus Hrachowitz[2], Michael Stockinger[1], Paul Koeniger[3], Siyuan Wang[4], and Christine Stumpp[1]

[1]BOKU University, Institute of Soil Physics and Rural Water Management, Department of Landscape, Water and Infrastructure, 1190 Vienna, Austria
[2]Department of Water Management, Faculty of Civil Engineering and Geosciences, Delft University of Technology, 2628CN Delft, the Netherlands
[3]Groundwater Resources, BGR Federal Institute for Geosciences and Natural Resources, 30655 Hannover, Germany
[4]Water, Energy and Environmental Engineering, University of Oulu, 90014 Oulu, Finland

Correspondence to: Karl Knaebel (karl.knaebel@boku.ac.at)

Abstract. Water-age dynamics have been widely investigated in small- to meso-scale catchments using transit-time distributions (TTDs) and water-age fractions but remain poorly quantified in large river basins. Because large river basins integrate heterogeneous landscapes, tributaries, and storage domains, it remains unclear how their water-age dynamics compare with those of smaller catchments. Here, based on 20 years of $\delta^{18}O$ in streamflow data and linked to hydroclimatic data from six large Central European river basins (4,981–131,950 km²), we implemented a semi-distributed, tracer-aided conceptual hydrological model coupled with StorAge Selection (SAS) functions and computed time-variable TTDs and derived numerous water-age fractions including f_{30} ($t \leq 30$ days), f_{90} ($t \leq 90$ days). Specifically, we (i) quantified and compare TTDs and water-age fractions under high-, intermediate-, and low-flow conditions; (ii) assessed their intra-annual variability within each flow condition; and (iii) identified hydroclimatic controls on water-age fractions. We found substantial young water contributions in all six basins, with median f_{90} ranging from 0.23 to 0.35 among basins. During high flows, median f_{90} values ranged from 0.30 to 0.51 among basins, with a cross-basin median of 0.42 that was 1.7 and 2.8 times as high as during intermediate and low flows, respectively. However, discharge-age sensitivities differed substantially among basins ranging from relatively stable water-age compositions across flow conditions in some basins to markedly stronger shifts between younger and older water contributions in others i.e., median f_{90} during high flows was ranging from 1.5 to 8 times as high as under low flow conditions. Seasonal contrasts in younger water-age fractions were pronounced during high and intermediate flows but weak during low flows. During high flows, median f_{30} was 0.42 in summer and 0.36 in autumn, compared with 0.21 in winter and 0.14 in spring across basins and median f_{90} was 0.51 in autumn versus 0.32 in spring. Water-age fractions varied substantially among basins and across flow conditions and seasons. Among the hydroclimatic variables tested, modelled discharge and the Standardized Precipitation Evapotranspiration Index based on the preceding 30 days ($SPEI_{30}$) explained merely part of this variability. Overall, our findings challenge the common intuition that streamflow

https://doi.org/10.5194/egusphere-2026-6810
Preprint. Discussion started: 25 November 2026
© Author(s) 2026. CC BY 4.0 License.



in large river basins may be dominated by older water, as all six basins showed substantial younger-water contributions that were comparable to or even higher than those reported for small- to meso-scale catchments and were especially pronounced under high flows.

1 Introduction

Climate change is increasing the frequency and severity of hydrological extremes, including floods and droughts, with major implications for river systems and water-resources management (Hakala et al., 2019; Intergovernmental Panel on Climate Change, 2023). Such extremes can alter hydrological connectivity, catchment storage, flow paths and thereby influence the mobilization, transport, and transformation of solutes, nutrients, and pollutants (van der Velde et al., 2015; Fovet et al., 2015; Hrachowitz et al., 2016). Assessing these impacts requires approaches that go beyond quantifying changes in streamflow alone and instead examine how water storage, mixing, and release processes within a catchment shape streamflow. Stable water isotopes in precipitation and streamflow, specifically ^{2}H and ^{18}O, provide a powerful tool for investigating these processes, in particular when measured over long time periods. As the isotopic signal of precipitation varies with season and is modified by storage and mixing within catchments, stable isotopes can be used as tracers to infer water ages. The latter are a powerful tool to determine water sources and flow paths, which, in turn, are a major control on nutrient and pollutant circulation (Sprenger et al., 2019). As water age cannot be measured directly, various metrics of the water age of streamflow were developed, such as the proportion of event and pre-event water, the fraction of young water (f_{yw}; Kirchner, 2016a), or in general the mean transit time (MTT) and the transit time distributions (TTDs). These metrics can be estimated using isotope-enabled methods, including ensemble hydrograph separation (Klaus and McDonnell, 2013), sine-wave approaches (Małoszewski et al., 1983; DeWalle et al., 1997) or convolution-integral models (Małoszewski and Zuber, 1982), and more recently, StorAge Selection (SAS) functions (Rinaldo et al., 2015) and their coupling with hydrological models (Birkel and Soulsby, 2015; Stadnyk and Holmes, 2023).

As a descriptor of water age, TTDs provide a framework for characterizing how catchments store, mix, and release water under variable and changing hydroclimatic conditions. TTDs describe the distribution of times that water parcels spend within a catchment between entering as precipitation and leaving as streamflow or evapotranspiration. Over the past decades, it has been increasingly acknowledged that TTDs are dynamic rather than static (e.g., McGuire and McDonnell, 2006; McDonnell et al., 2010; Benettin et al., 2022). While previous studies focused on long-term descriptors such as mean or median time-invariant TTD, the focus has shifted towards approaches that resolve TTDs and related metrics in a time-variable manner. This development reflects the understanding that stream water ages vary with streamflow, hydroclimatic forcing, antecedent wetness, storage state, and the activation or deactivation of flow paths allowing to infer the TTDs in a time-variable way (e.g., Botter et al., 2011; Hrachowitz et al., 2013; Benettin et al., 2022; Wang et al., 2025). Under wet conditions, enhanced hydrological connectivity and the activation of shallow, fast flow paths often increase the contribution of f_{yw} in streamflow (e.g., von Freyberg et al., 2018; Yang et al., 2021; Floriancic et al., 2024; Türk et al., 2025). Conversely,

https://doi.org/10.5194/egusphere-2026-6810
Preprint. Discussion started: 25 November 2026
© Author(s) 2026. CC BY 4.0 License.

under dry conditions, shallow fast pathways may become disconnected, and streamflow is often sustained by older water released from groundwater or larger storage domains (e.g., Morgenstern et al., 2010; Hrachowitz et al., 2015; Hrachowitz et al., 2021). Consequently, stream water age varies systematically with discharge: high flows, typically associated with wet conditions, generally comprise younger water, whereas low flows during dry periods are more strongly influenced by older water. During high flows, f_{yw} generally increases as faster flow paths become more important, and young water can dominate streamflow during flood events (e.g., Kirchner, 2016b; von Freyberg et al., 2018; Gallart et al., 2020; Hachgenei et al., 2024). In contrast, during low-flow and drought conditions, mean transit times tend to increase substantially, indicating a greater contribution of older water (e.g. Morgenstern et al., 2010; Cartwright and Morgenstern, 2015). This strong flow dependence is consistent with studies based on the SAS approach showing that the composition of discharge may shift from the preferential release of younger water during wet periods towards the release of older water during drying and dry periods, reflecting seasonal changes in dominant flow paths and catchment connectivity (e.g., Wilusz et al., 2017; Rodriguez et al., 2018; Rodriguez et al., 2021; Türk et al., 2026b).

Most of the understanding of TTDs and water-age dynamics has been developed in headwater, experimental, or small- to meso-scale catchments, where high-resolution tracer data and detailed process observations are often available (e.g., Pearce et al., 1986; Sklash et al., 1986; McDonnell, 1990; Sklash et al., 1996; Benettin et al., 2015a; Benettin et al., 2015b). Such studies have provided essential insights into catchment storage, mixing, and release processes, but they offer limited evidence for how water-age dynamics scale to large river basins. Large basins integrate spatially heterogeneous climates, physiography, land use, groundwater systems, storage domains, and tributary networks, and may therefore exhibit water-age dynamics that differ from those observed in smaller systems. Across large Central European basins, previous studies have characterized spatial and seasonal variability in isotopic composition (Reckerth et al., 2017) whereas others have quantified individual water-age metrics, such as the fraction of young water (Stockinger and Stumpp, 2024). Although recent studies have started to apply time-variable TTDs approaches to larger spatial domains (e.g., Wang et al., 2023), explicitly time-variable applications over long periods and at large-scale remain rare.

This highlights two important research gaps: a systematic investigation of TTDs, and a quantification of how they vary under high-flow and low-flow conditions in large-scale basins. Consequently, systematic analyses at these large scales are needed to test whether conceptual understanding derived mainly from small and meso-scale catchments holds to investigate TTDs of variable flow conditions at the larger river basin scale. In this study, we therefore investigate TTDs and derived water-age fractions across six large Central European river basins ranging from 4,981 to 131,950 km^2, by implementing a semi-distributed conceptual tracer-aided hydrological model utilizing 20 years of hydro-meteorological and $\delta^{18}O$ data. The objectives of this study were: (i) to determine and compare TTDs and derived water-age fractions for high-, intermediate-, and low-flow conditions; (ii) to investigate the intra-annual variability of TTDs and water-age fractions within these flow conditions; and (iii) to explore hydroclimatic controls on water-age fraction across large river basins. This study provides new insight into how large river basins store and release water under contrasting extreme hydrological conditions.

https://doi.org/10.5194/egusphere-2026-6810
Preprint. Discussion started: 25 November 2026
© Author(s) 2026. CC BY 4.0 License.

2 Study area

We investigated six large-scale, Central European river basins ranging from 4,981 km^2 – 131,950 km^2 with a combined area of 311,057 km^2 (Fig. 1). The study basins, and stream-water $\delta^{18}O$ sampling sites given in brackets, were the Elbe (Geesthacht), Ems (Geeste), Main (Eddersheim), Moselle (Koblenz), Neckar (Schwabenheim), and Oder (Schwedt). Discharge gauging stations were selected by minimizing the distance to the upstream isotope ($\delta^{18}O$) sampling sites (Tab. 1). The studied basins span a broad physiographic gradient, from flat northern basins (Elbe, Oder, Ems) to central and southern basins shaped by uplands and low mountain ranges (Moselle, Neckar, Main). Across these basins, mean annual precipitation is ~584–834 mm yr^{-1}, mean annual potential evapotranspiration is 775–835 mm yr^{-1}, mean annual discharge is 155–343 mm yr^{-1}, and mean annual air temperature is 9.2–10.4 °C for the period 2001–2020 (Tab. 1). Based on CORINE Land Cover data (EEA, 2020), the combined catchment area averages 56 % agriculture, 33 % forest, 8 % urban areas, 1 % open water, and 2 % other.

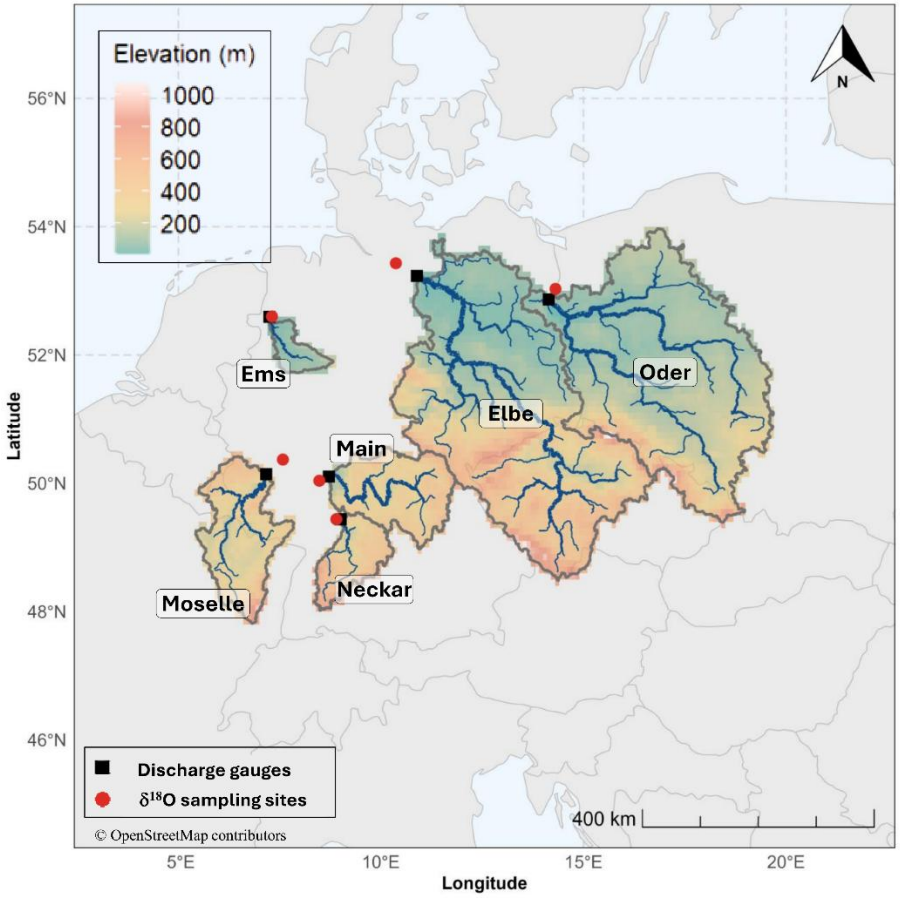

Figure 1: Study area with the six basins Elbe, Ems, Moselle, Main, Neckar, and Oder with respective discharge gauges and $\delta^{18}O$ sampling locations. Data Source: © OpenStreetMap contributors; elevation data from GTOPO30; river network data from HydroSHEDS (Lehner and Grill, 2013); and basin boundaries supplied alongside streamflow data by the Global Runoff Data Centre (GRDC), Federal Institute of Hydrology (BfG).

https://doi.org/10.5194/egusphere-2026-6810
Preprint. Discussion started: 25 November 2026
© Author(s) 2026. CC BY 4.0 License.

Table 1: $\delta^{18}O$ river sampling sites and discharge gauging station with total basin area, mean elevation and elevation range, forested- and agricultural area in % for the six river basins. We selected the closest downstream discharge station relative to the river water isotope sampling sites. Long-term mean annual observed (Q) and modelled discharge (Q_m), precipitation (P), potential evapotranspiration (Ep) in mm yr-1 and annual mean temperature (T) in °C were calculated based on the period 2001-2020.

Catchment	$\delta^{18}O$ sampling sites	Lat (°)	Long (°)	Discharge gauging stations	Lat (°)	Long (°)	Area (km^2)	Elevation mean (m)	Elevation range (m)	Q (mm yr^{-1})	Q_m (mm yr^{-1})	P (mm yr^{-1})	Ep (mm yr^{-1})	T (°C)	Forest (%)	Arable land (%)
Elbe	Geestacht	53.43	10.34	Neu Darchau	53.23	10.88	131,950	289	12 – 1,115	155	143	627	798	9.2	31.1	56.9
Ems	Geeste	52.60	7.25	Dalum	52.60	7.24	4,981	76	22 – 266	281	272	754	775	10.4	12.4	74.9
Main	Eddersheim	50.02	8.45	Frankfurt Osthafen	50.10	8.71	24,764	371	113 –747	224	229	740	820	9.3	40.2	51.1
Moselle	Koblenz	50.14	7.17	Cochem	50.14	7.16	27,088	355	171 – 960	343	335	834	817	10.0	37.4	51.8
Neckar	Schwabenheim	49.44	9.01	Rockenau Ska	49.43	9.00	12,710	472	188 – 893	314	327	829	835	9.5	36.7	50.4
Oder	Schwedt	53.04	14.31	Hohensaaten -Finow	52.86	50.44	109,564	178	5 – 1,115	131	124	584	793	9.2	32.6	56.9

https://doi.org/10.5194/egusphere-2026-6810
Preprint. Discussion started: 25 November 2026
© Author(s) 2026. CC BY 4.0 License.

3 Data

3.1 Hydro-meteorological data

Daily meteorological data from the E-OBS dataset (version 30.0e; 0.1° regular grid; DOI: 10.24381/cds.151d3ec6) were used for the period 1 January 1950 to 31 December 2020 (Cornes et al., 2018). We used the daily mean, maximum and minimum air temperature (°C) and daily precipitation (mm d^{-1}). Daily potential evapotranspiration E_p (mm d^{-1}) was calculated from the daily mean, maximum and minimum temperature using Hargreaves method via the pyet Python library (Vremec et al., 2024). Daily mean river discharge (m^3 s^{-1}) for the individual discharge gauging locations (Fig. 1 and Tab. 1), provided by the German Federal Institute of Hydrology (BfG), was downloaded for the period 1960 – 2020 from the Global Runoff Data Centre (GRDC; https://grdc.bafg.de/) and the EStreams data portal (https://www.estreams.eawag.ch/; do Nascimento et al., 2024). Discharge observations were normalized by catchment area and converted to runoff depth (mm d^{-1}). Throughout this study, the terms "streamflow" and "discharge" are used interchangeably to refer to this normalized variable. MODIS/Terra Snow Cover 8-Day L3 Global 500 m product (MOD10A2, Collection 6.1; Hall and Riggs, 2021; DOI: 10.5067/MODIS/MOD10A2.061) was retrieved for the study area via Google Earth Engine (GEE) for the period February 2000 to December 2020. This product provides the maximum observed snow extent for each 8-day composite period. Elevation data were derived from the Global 30 Arc-Second Elevation (GTOPO30) dataset, provided as an ancillary file on a 0.1° regular grid with E-OBS.

3.2 Stable isotope data

Mean monthly $\delta^{18}O$ in streamflow was available from Reckerth et al. (2017), Koeniger et al. (2022) and from the German Isotope Network (GIN; https://www.isotopes-GIN.de). The isotope sampling sites and their closest associated discharge stations are listed in Tab. 1. As described by Reckerth et al. (2017), river water was sampled using automatic samplers (SP III-XY-36, Maxx Mess- und Probenahmetechnik GmbH). Each sampler held 36 × 2.5 L bottles and every 30 min an amount of 50 mL was collected, i.e., 48 subsamples filling one bottle per day. Daily bottles were pooled into monthly composite samples, reflecting the non-flow-weighted monthly mean isotopic composition. The $\delta^{18}O$ isotope ratio was analyzed with dual-inlet mass spectrometry and laser-based cavity ring-down spectrometers (L2120-i/L2130-i, Picarro Inc.), with a precision better than ±0.2 ‰. Analysis was conducted at the GSF Helmholtz Center Neuherberg/Munich until 2016 and from 2017 onwards at the BGR Federal Institute for Geosciences and Natural Resources, in Hannover, Germany. Modelled monthly $\delta^{18}O$ in precipitation were available from the machine learning framework "Piso.Ai" (version 1.01; https://isotope.bot.unibas.ch/PisoAI/), i.e. a gridded product at a resolution of 0.5° for the period January 1980 – December 2020 (Nelson et al., 2021). All $\delta^{18}O$ values are given in per mil (‰) relative to the Vienna Standard Mean Ocean Water (V-SMOW).

https://doi.org/10.5194/egusphere-2026-6810
Preprint. Discussion started: 25 November 2026
© Author(s) 2026. CC BY 4.0 License.

4 Methods

4.1 Tracer-aided hydrological model

We implemented a tracer-aided hydrological model similar to Wang et al. (2023) and Türk et al. (2025) by coupling a hydrological model built on the DYNAMIT framework (Hrachowitz et al., 2013; Hrachowitz et al., 2021) with a tracer transport model that employs StorAge Selection (SAS) functions (Rinaldo et al., 2015). The model runs at a daily time-step and predicts streamflow and $\delta^{18}O$ in streamflow, enabling the estimation of time-variable TTDs and derived water-age fractions.

4.1.1 Hydrological model

The hydrological modelling scheme comprises five conceptual reservoirs: snow storage, canopy interception, the unsaturated root-zone storage, a fast-response storage, and a slow-response storage subdivided into active and passive components (see Fig. 2). To better capture hydrograph attenuation in large basins, we augmented the modelling scheme with a triangular river routing function similar to the MAXBAS transfer-function of the HBV model (Bergström, 1992). Following a parcel of water from precipitation to evaporation or streamflow: daily precipitation P (mm d^{-1}) is partitioned into snowfall P_{snow} (mm d^{-1}) and rainfall P_{rain} (mm d^{-1}) using a threshold temperature parameter T_t (°C), with snowfall for $T \leq T_t$ and rainfall for $T > T_t$ (Gao et al., 2017). Snowfall accumulates in the snow storage S_{snow} (mm) and snowmelt M_{snow} (mm d^{-1}) is computed using a degree-day method parameterized by the melt factor C_{melt} (mm d^{-1} $°C^{-1}$), which is applied when $T>T_t$ (Prenner et al., 2018; Girons Lopez et al., 2020). P_{rain} enters the interception storage S_i (mm). Evaporation from S_i occurs at E_i (mm d^{-1}). When S_i reaches the maximum interception storage capacity S_{imax} (mm), any excess forms net precipitation P_n (mm d^{-1}; e.g. Nijzink et al., 2016). M_{snow} or P_n enter the unsaturated storage S_u (mm) as effective precipitation P_e (mm d^{-1}). From S_u water is released to the atmosphere as a combined soil evaporation and transpiration flux E_a (mm d^{-1}). Liquid drainage from S_u either recharges the active groundwater storage S_s (mm) as percolation R_{perc} and faster preferential recharge R_{pref} (mm d^{-1}) or is routed as R_{uf} (mm d^{-1}) to the fast storage S_f (mm). Generated discharge Q_g (mm d^{-1}) is then computed by combining the lateral preferential flow Q_f (mm d^{-1}) from S_f and baseflow Q_s (mm d^{-1}) from S_s. Finally, Q_g is routed with a triangular routing kernel parameterized by the time-to-peak T_p producing modelled discharge Q_m (mm d^{-1}). The detailed model equations can be found in Tab. S1 and Tab. S2 in the supplementary material.

https://doi.org/10.5194/egusphere-2026-6810
Preprint. Discussion started: 25 November 2026
© Author(s) 2026. CC BY 4.0 License.

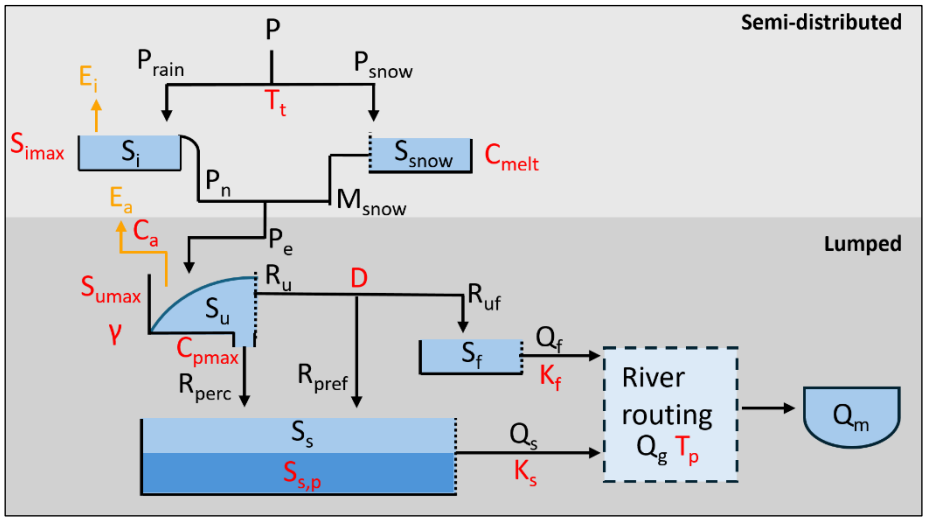

Figure 2: Structure of the implemented hydrological model. Semi-distributed reservoirs represent interception storage (S_i) and snow storage (S_{snow}), while lumped reservoirs represent the unsaturated storage (S_u), active and passive groundwater storages (S_s and $S_{s,p}$), fast storage (S_f), and river routing. Black lines indicate water fluxes, orange lines indicate evaporation fluxes, and red labels denote model parameters. Abbreviations are defined in section 4.1.1, and the governing equations are provided in the Supplement. The model is augmented with StorAge Selection (SAS) functions to simultaneously simulate water fluxes and $\delta^{18}O$ as outlined in section 4.1.2.

4.1.2 Tracer transport model

To account for $\delta^{18}O$ transport, the hydrological model was extended with SAS functionality (Rinaldo et al., 2015). In summary, at any given time t (d), each storage reservoir j stores water of different ages denoted by T (d) which are linked to past precipitation and ranked by input time, forming the age-ranked water storage $S_{T,j}(T,t)$ (Harman, 2015; Benettin et al., 2017). Then, the distribution of water of different ages in storage is called $p_s(T,t)$ and is in its cumulative form referred to as the cumulative residence time distribution (RTD). The residence time distribution depends on the sequence of past inflows $I_j(t)$ and outflows $O_j(t)$ and varies over time. Accordingly, the water age distribution of any outflow stated as $p_{O,T}(T,t)$ is time-variable as well and is in its cumulative form named the cumulative transit time distribution (TTD). RTD and TTD are linked via the SAS function ω, which defines the water release from storage by water age. Each storage reservoir is assumed to be well mixed, with a uniform SAS function (ω = const) i.e., outflows are sampled uniformly across water ages (Birkel et al., 2011; van der Velde et al., 2015; Rodriguez et al., 2018). Given that the actual shapes of SAS functions in each storage component are a priori unknown (Türk et al., 2026a), the use of uniform SAS functions for the individual storage reservoirs represents a pragmatic assumption for large-scale application balancing process heterogeneity and epistemic uncertainty. For each storage reservoir j (e.g., S_{snow}, S_u), the age-ranked storage is updated at time t while conserving water ages by Eq. 1 (Botter et al., 2011; van der Velde et al., 2012; Harman, 2015)

https://doi.org/10.5194/egusphere-2026-6810
Preprint. Discussion started: 25 November 2026
© Author(s) 2026. CC BY 4.0 License.

$$\frac{\partial S_{T,j}(T,t)}{\partial t} + \frac{\partial S_{T,j}(T,t)}{\partial T} = \sum_{n=1}^{N} I_{T,n,j}\,(T,t) - \sum_{m=1}^{M} O_{T,m,j}\,(T,t) \tag{1}$$

where: $\partial S_{T,j}(T,t)/\partial t$ denotes the temporal change in age-ranked storage and $\partial S_{T,j}(T,t)/\partial T$ aging within storage; the evolution of $S_{T,j}(T,t)$ is governed by age-ranked inflows $I_{T,n,j}\,(T,t)$ and outflows $O_{T,m,j}\,(T,t)$ for reservoir j; N and M denote the number of inflow and outflow terms, respectively (e.g., M_{snow} and P_n as inflows, and E_a, R_u, and R_{perc} as outflows of S_u). Next (Eq. 2), for each storage reservoir j, the age-ranked outflow $O_{T,m,j}\,(T,t)$, i.e., the TTD, depends on the outflow volume $O_{m,j}(t)$, estimated from the hydrological model and the cumulative age distribution of that outflow $P_{o,m,j}(T,t)$:

$$O_{T,m,j}\,(T,t) = O_{m,j}\,(t)\;P_{o,m,j}\,(T,t) \tag{2}$$

where $P_{o,m,j}\,(T,t)$ is a function of the cumulative age distribution at t of the storage reservoir $S_{T,j}\,(T,t)$ and the SAS function $\Omega_{o,m,j}$ and can be expressed as Eq. 3:

$$P_{o,m,j}\,(T,t) = \Omega_{o,m,j}\,(S_{T,j}\,(T,t),t) \tag{3}$$

with $\Omega_{o,m,j}$ being the cumulative form of $\omega_{o,m,j}$. Consequently, the probability density function of any outflow linked with the cumulative distribution $P_{o,m,j}\,(T,t)$ can be formulated as Eq. 4:

$$p_{o,m,j}\,(T,t) = \omega_{o,mj}\,(S_{T,j}\,(T,t),t)\,\frac{\partial S_{T,j}}{\partial T} \tag{4}$$

where $\omega_{o,mj}$ is the probability density function i.e., the SAS function. To prevent rescaling the SAS function at every time step, we normalized the age-ranked storage $S_{T,j}\,(T,t)$ by its total volume $S_j(t)$ as in Eq. 5:

$$S_{T,norm,j}\,(T,t) = \frac{S_{T,j}(T,t)}{S_j(t)} \tag{5}$$

with $0 \le S_{T,norm,j} \le 1$.

Alongside the groundwater storage S_s, the passive groundwater storage denoted as $S_{s,p}$ (mm) describes the groundwater volume below the riverbed (e.g., Zuber, 1986; Fenicia et al., 2010; Birkel et al., 2011; Hrachowitz et al., 2016). $S_{s,p}$ is

https://doi.org/10.5194/egusphere-2026-6810
Preprint. Discussion started: 25 November 2026
© Author(s) 2026. CC BY 4.0 License.

hydrologically inactive ($dS_{s,p}/dt = 0$), i.e., the baseflow Q_s is exclusively governed by the time-varying S_s. $\delta^{18}O$ and the age composition of Q_s are sampled from the combined storage denoted as $S_{s,\mathrm{tot}} = S_s + S_{s,p}$ to attenuate the tracer input variability. Finally, $\delta^{18}O$ is routed through all the reservoirs, and the tracer concentration of each outflow m is computed by Eq. 6 (Harman, 2015; Benettin et al., 2017)

$$C_{o,m,j}(t) = \int_0^{S_j} C_{s,j}\left(S_{T,j}(T,t),t\right)\,\omega_{o,m,j}\left(S_{T,j}(T,t),t\right)\,dS_T \tag{6}$$

with $C_{o,m,j}$ denoting the tracer concentration in outflow m from storage component j at time t, and $C_{s,j}$ denotes the tracer concentration of water in storage component j at time t.

4.2 Semi-distributed model setup

To balance spatial detail with available data for model calibration, parameter identifiability and computational cost, we implemented a parsimonious semi-distributed model setup (Fig. 2). Therefore, each river basin was stratified into 200 m elevation zones based on the Global 30 Arc-Second Elevation Data Set (GTOPO30) provided in E-OBS. The elevation-zone ranges and their respective fractions of the total basin area are provided in Tab. S3 of the supplementary material. Snow and interception storages were represented separately for each elevation zone (e.g., Mostbauer et al., 2018), whereas all other storages were represented lumped in an approach similar to Euser et al. (2015). Previously, Wang et al. (2023) found comparable model performance and water-age estimates for lumped and semi-distributed model implementations in the Neckar catchment, supporting our decision to represent all model reservoirs except snow and interception storages as lumped. Hence, E-OBS meteorological forcing data and Piso.Ai precipitation $\delta^{18}O$ data were aggregated for each elevation zone by averaging the corresponding grid cells, resulting in distinct forcing time series for each elevation zone. Modelled outflows from each elevation zone (e.g., E_i, M_{snow} and P_e) were aggregated calculating the area-weighted average across elevation zones and then routed to the unsaturated root-zone storage S_u. The model setup comprised 13 parameters (Fig. 2, with model parameters shown in red), which were calibrated and tested separately for each river basin.

4.3 Model calibration and testing

Model calibration was performed for the period from October 2001 to December 2020 against daily streamflow observations and the complete available $\delta^{18}O$ in streamflow record. We included all $\delta^{18}O$ observations in the calibration rather than dividing the $\delta^{18}O$ time series into separate calibration and testing periods, ensuring that the $\delta^{18}O$ data covered the widest possible range of hydrological conditions, including both high- and low-flow periods (e.g., Arsenault et al., 2018; Shen et al., 2022). Modelled streamflow was compared with daily observations, while modelled daily $\delta^{18}O$ in streamflow were aggregated to monthly non-flow-weighted mean values and compared with observed monthly mean $\delta^{18}O$ values. TTDs and

https://doi.org/10.5194/egusphere-2026-6810
Preprint. Discussion started: 25 November 2026
© Author(s) 2026. CC BY 4.0 License.

water-age fractions were therefore derived only for the calibration period and describe catchment behaviour under the observed conditions, not predictions beyond it. Additionally, we tested the model against streamflow observations from an independent period preceding the calibration period, spanning 1960/1970 to 1980, depending on data availability of each river basin. Both calibration and test periods were preceded by model warm-up periods. The detailed calibration and test periods for each river basin are provided in the supplementary material Tab. S4. Each river basin was simultaneously calibrated against seven performance measures based on the mean square error (MSE) of six streamflow signatures and one $\delta^{18}O$ signature, which were combined in a multi-objective function (Eq. 7) using the Euclidian distance D_E (e.g., Wang et al., 2023)

$$D_E = \sqrt{\frac{1}{2}\left(\frac{\sum_{n=1}^{N}(MSE_{Q,n})^2}{N} + MSE_{\delta 18O}{}^2\right)} \quad (7)$$

with N = 6 being the number of streamflow MSEs i.e., streamflow and logarithmic streamflow (MSE_Q and $MSE_{log(Q)}$), autocorrelation (MSE_{ACQ}), seasonal runoff coefficient (MSE_{RC}), the flow duration curve (MSE_{FDCQ}), the logarithmic flow duration curve ($MSE_{FDClog(Q)}$) as well as the MSE of $\delta^{18}O$ in streamflow ($MSE_{\delta 18O}$). Pareto optimal parameter sets were identified using differential evolution (Storn and Price, 1997), minimizing D_E, where $D_E = 0$ denotes a perfect model fit. The initial population was generated using Latin hypercube sampling (Vořechovský, 2015) within the specified parameter bounds. Initial parameter bounds as well as the parameter ranges for the top 20 % of Pareto-optimal parameter sets are listed in the supplementary material for all river basins in Tab. S5. We computed Nash–Sutcliffe model efficiency coefficients (NSE) for streamflow and tracer signatures to further evaluate the model (Nash and Sutcliffe, 1970). TTDs and derived water-age fractions (see section 4.5) were computed in the calibration period using the parameter set with the lowest D_E. All results presented in this study were derived from the calibration period.

4.4 Evaluation of modelled snow storage

Additionally, we evaluated the modelled snow storage against MODIS/Terra maximum snow extent observations following the work of Parajka and Blöschl (2008) and Tong et al. (2022). The evaluation was conducted for all river basins from February 2000 to December 2020. Within each basin, MODIS/Terra 8-day snow extent composites were compared with modelled snow cover separately for each elevation zone. The MOD10A2 composites were first reclassified in Google Earth Engine into three classes: snow covered, snow free, and cloud cover/no data. The reclassified composites were subsequently aggregated by elevation zone to derive time series of the percentage snow-covered area (SCA), snow-free area, and cloud-covered area. Following the thresholds of Parajka and Blöschl (2008), only elevation-zone composites with cloud coverage below 60 % were retained for evaluation. An elevation zone was classified as snow covered when its snow-covered area exceeded 25 % of the elevation-zone area (SCA > 25 %). Modelled snow cover was classified as present when $S_{snow} > 0$ mm.

https://doi.org/10.5194/egusphere-2026-6810
Preprint. Discussion started: 25 November 2026
© Author(s) 2026. CC BY 4.0 License.

The snow-cover error (S_E) was computed per elevation zone as the sum of the model overestimation (S_{snow} > 0 mm and SCA ≤ 25 %) and underestimation (S_{snow} = 0 mm and SCA > 25 %). For each river basin, the overall snow-cover error was calculated as the area-weighted average of all elevation zone. The detailed equations are provided in the Supplementary Information Tab. S6.

4.5 TTD derived water-age fractions

We computed the TTD of streamflow at the daily time step as described in Section 4.1.2 and, derived the following water-age fractions at the same resolution: f_{10} the fraction of streamflow younger than 10 days (t≤10 days), f_{30} the fraction of streamflow younger than 30 days (t≤30 days), f_{90} the fraction of streamflow younger than 90 days (t≤90 days), f_{1yr} the fraction of streamflow younger than one year (t≤1 year), f_{5yr} the fraction of streamflow younger five years (t≤5 years), f_{older} the fraction of streamflow older than five years f(t>5 years).

4.6 Data analysis

For all river basins a detailed data analysis was conducted for the period October 2001 until December 2020. We defined high, intermediate and low flow conditions based on modelled discharge (Q_m) using exceedance quantiles derived from the calibration period: high ($Q_m > Q_{m,10}$), intermediate ($Q_{m,90} \leq Q_m \leq Q_{m,10}$), and low ($Q_m < Q_{m,90}$) (e.g., Sawicz et al., 2014). We used modelled discharge Q_m to classify flow conditions rather than the observed streamflow because it is consistent with the model's internal water balance and the modelled TTDs and derived water-age fractions. To evaluate the model's ability to reproduce these conditions, we used two complementary metrics. First, to assess the accuracy of the modelled quantile thresholds, we calculated ΔQ_p, representing the difference between modelled and observed flow values at a given exceedance percentile p on the flow-duration curve (Eq. 8).

$$\Delta Q_p = 100 \frac{Q_{m,p} - Q_p}{Q_p} \tag{8}$$

where $Q_{m,p}$ is the modelled flow value that is exceeded for p percent of the time, and Q_p is the corresponding observed value. We applied this metric for both the high-flow (p=10) and low-flow (p=90) thresholds. Second, to quantify the average volumetric bias within the different flow conditions, we calculated Percent Bias (PBIAS; Eq. 9).

$$PBIAS = 100 \frac{\sum_{i=1}^{n}(Q_i - Q_{m,i})}{\sum_{i=1}^{n} Q_i} \tag{9}$$

https://doi.org/10.5194/egusphere-2026-6810
Preprint. Discussion started: 25 November 2026
© Author(s) 2026. CC BY 4.0 License.

where Q is the observed streamflow and Q_m is the corresponding modelled streamflow. PBIAS was computed separately for the high-flow (PBIAS-H), intermediate (PBIAS-I), and low-flow (PBIAS-L) conditions. However, it should be kept in mind that streamflow observations are themselves subject to uncertainty, particularly during low- and high-flow conditions (McMillan et al., 2012; Kiang et al., 2018). We defined seasons following the standard meteorological definitions: winter (December–February), spring (March–May), summer (June–August), and autumn (September–November). To distinguish between hydroclimatic wet and dry periods, we estimated the Standardized Precipitation Evapotranspiration Index (SPEI) (Vicente-Serrano et al., 2010). SPEI was estimated at the daily time step considering preceding 30, 90, and 365 days ($SPEI_{30/90/365}$) of precipitation and potential evapotranspiration, using the "climate_indices" Python library (v2.2.0; Adams, 2025). We performed a Spearman rank correlation analysis to investigate relationships between water-age fractions and a suite of hydroclimatic variables, including P, E_p, E_a, $SPEI_{30}$, $SPEI_{90}$, and $SEPI_{365}$, as well as Q_m. For each relationship, the Spearman correlation coefficient r_S and the associated p-value are reported, with statistical significance defined as $p < 0.05$. Theil-Sen slopes are reported for Q_m and $SPEI_{30}$, with denoting slopes whose 95 % confidence intervals exclude zero. Descriptive statistics are presented as medians with interquartile ranges (IQR; Q1–Q3) and as means with standard deviations (SD).

https://doi.org/10.5194/egusphere-2026-6810
Preprint. Discussion started: 25 November 2026
© Author(s) 2026. CC BY 4.0 License.

5 Results

5.1 Model performance

Model predictions of streamflow and $\delta^{18}O$ in streamflow were largely consistent with observations for all six basins (Fig. 3 and Fig. 4). Based on the best-performing parameter set (i.e., lowest D_E) for each basin, NSE $\delta^{18}O$ ranged from 0.59–0.76; NSE Q and NSE log(Q) ranged from 0.70–0.89 and 0.69–0.87, respectively, for the calibration period and from 0.66–0.87 and 0.63–0.87 for the test periods, respectively. Across all basins and for the best-performing parameter sets, the mean NSE Q and NSE log(Q) values were, respectively, 0.03 and 0.02 lower during the test period than during the calibration period. All performance metrics for the individual watersheds are given in Fig. 5. In terms of high and low flows averaged across all basins, the model exhibited a systematic negative bias in modelled streamflow, which was most pronounced under low-flow conditions. Although the model accurately reproduced the low-flow quantile Q_{90} on the flow-duration curve with a mean ΔQ_{90} of −2.7 %, it underestimated the magnitude of these low-flow periods, with a mean percent bias (PBIAS-L) of −25.5 % (equivalent to a mean error of −0.05 mm d^{-1}) across basins. High-flow performance was characterized by a moderate underestimation, with a mean ΔQ_{10} of −8.7 % and mean PBIAS-H −7.7 % (equivalent to a mean error of −0.12 mm d^{-1}) across basins. The PBIAS-I of intermediate flow conditions was minor, averaging 0.3 % across basins. Flow duration curves and associated PBIAS and ΔQ_{90} and ΔQ_{10} values, as well as the seasonal runoff coefficients of modelled versus observed values; and the complete observed and modelled time series of streamflow and $\delta^{18}O$ for individual river basins are presented in the Figures S1–S4 of the Supplementary Material. The fraction of precipitation falling as snow played a minor role in the study basins. Based on modelled precipitation partitioning, the long-term, elevation-zone area-weighted average fraction of precipitation falling as snow ranged from 1.9% in the Ems basin to 7.12 % in the Main basin. Evaluation of the modelled snow cover against MODIS/Terra observations revealed an elevation-zone area-weighted mean snow-cover error of 8.4 % across all river basins, with errors ranging from 6.9 % to 9.1 % among individual basins. Errors were nearly balanced, with modelled snow underestimation contributing an average error of 4.3 % and overestimation contributing 4.1 %. Snow-cover errors, including over- and underestimation errors for individual watersheds, are provided in Tab. S7 in the supplementary.

https://doi.org/10.5194/egusphere-2026-6810
Preprint. Discussion started: 25 November 2026
© Author(s) 2026. CC BY 4.0 License.

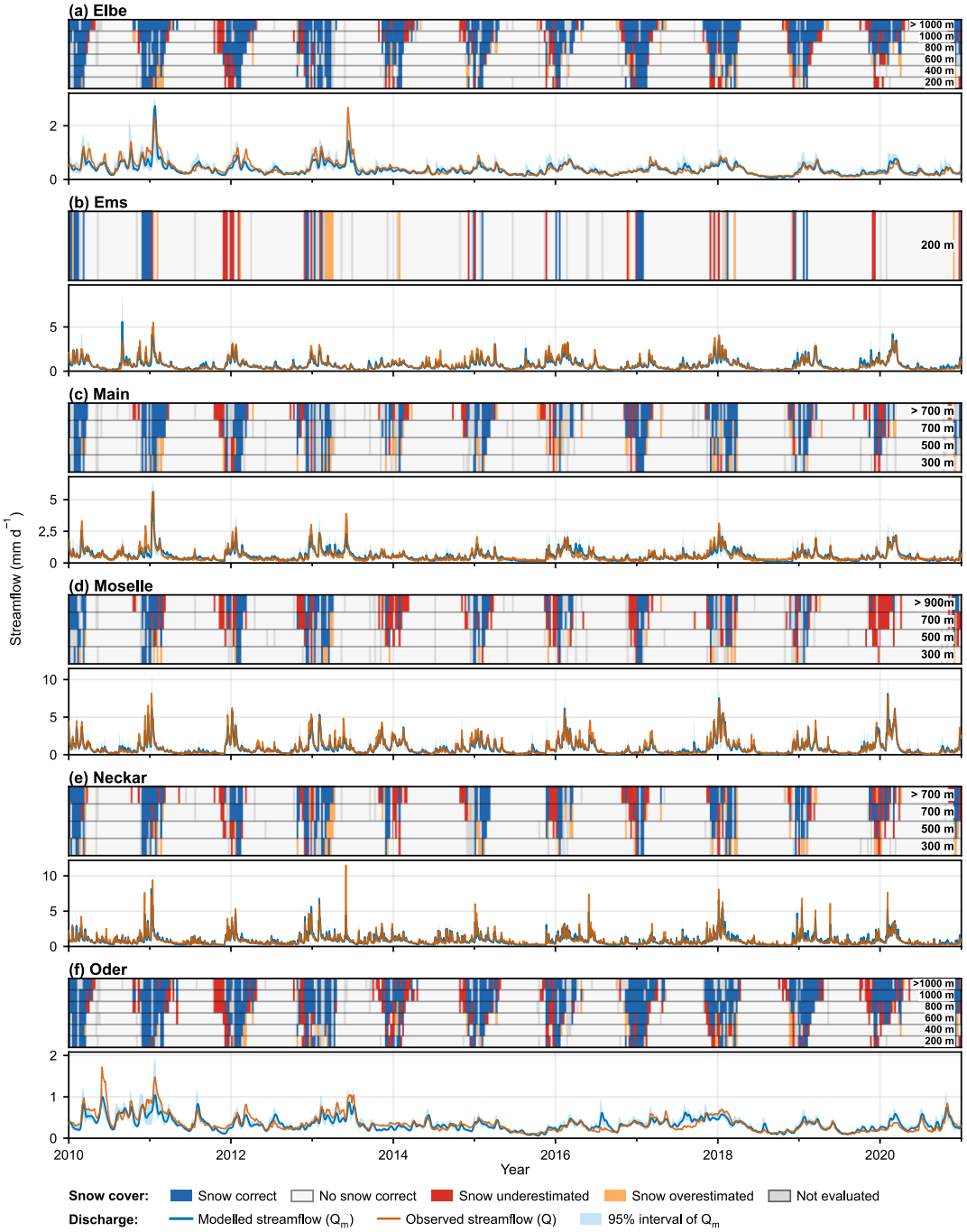

Figure 3: Streamflow model performance for the Elbe (a), Ems (b), Main (c), Moselle (d), Neckar (e), and Oder (f) basins during 2010–2020. For improved readability, each basin is shown separately. The upper panel presents simulated snow-cover conditions for the elevation zones, ordered from the lowest to the highest elevation. The lower panel compares observed and modelled daily streamflow. The model simulation with the lowest D_E is shown, and blue shaded bands indicate the central 95 % range of all retained Pareto-optimal solutions.

https://doi.org/10.5194/egusphere-2026-6810
Preprint. Discussion started: 25 November 2026
© Author(s) 2026. CC BY 4.0 License.

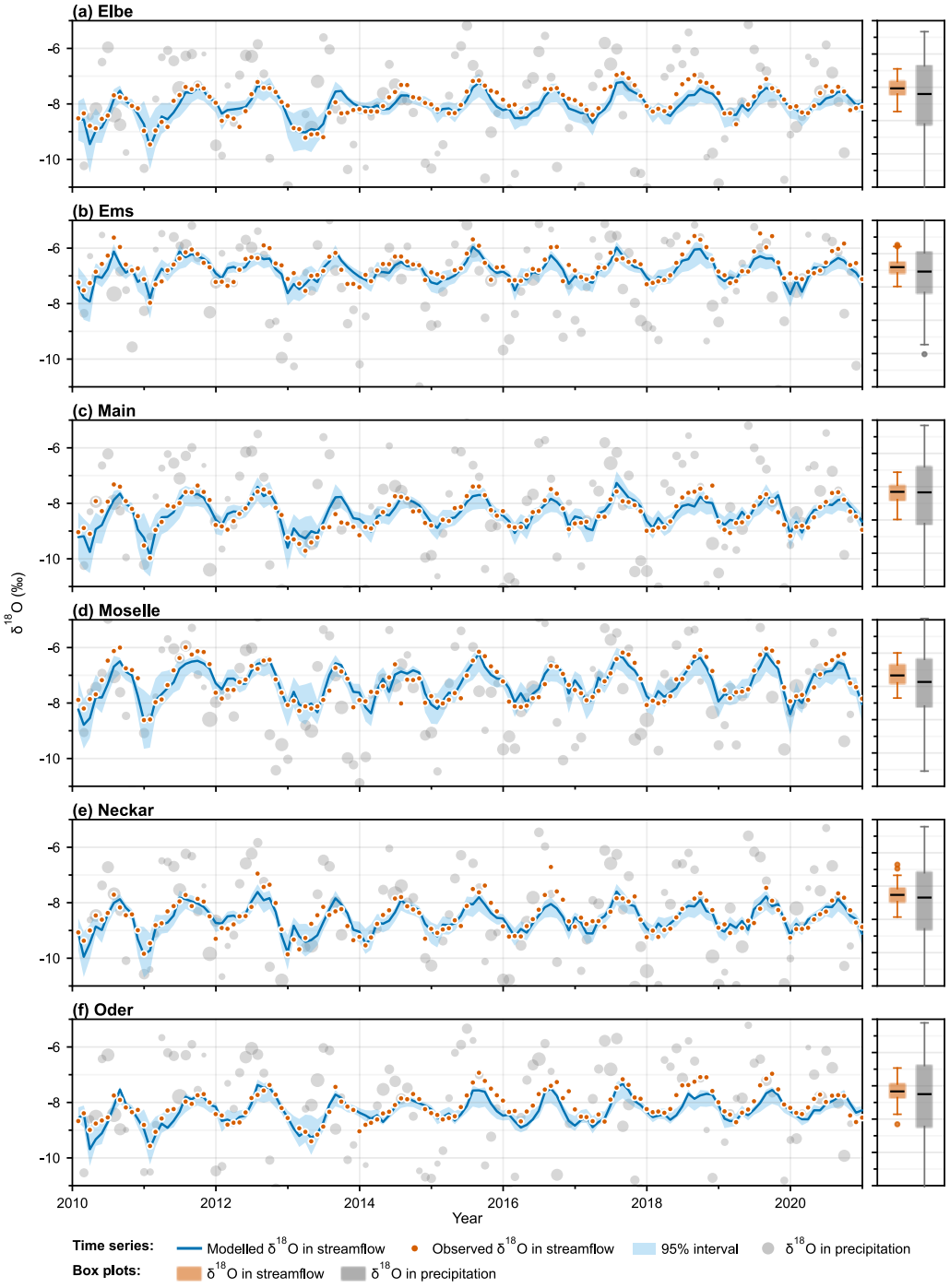

Figure 4: Performance of the $\delta^{18}O$ in streamflow for the Elbe (a), Ems (b), Main (c), Moselle (d), Neckar (e), and Oder (f) basins during 2010–2020. The time-series panels compare observed and modelled mean monthly $\delta^{18}O$ values in streamflow. $\delta^{18}O$ values in precipitation are shown as light-grey dots, with dot size indicating the relative precipitation volume. The boxplots compare $\delta^{18}O$ distributions in streamflow and precipitation over the full 2001–2020 period. The model simulation with the lowest D_E is shown, while blue shaded bands represent the central 95 % range of all retained Pareto-optimal solutions.

https://doi.org/10.5194/egusphere-2026-6810
Preprint. Discussion started: 25 November 2026
© Author(s) 2026. CC BY 4.0 License.

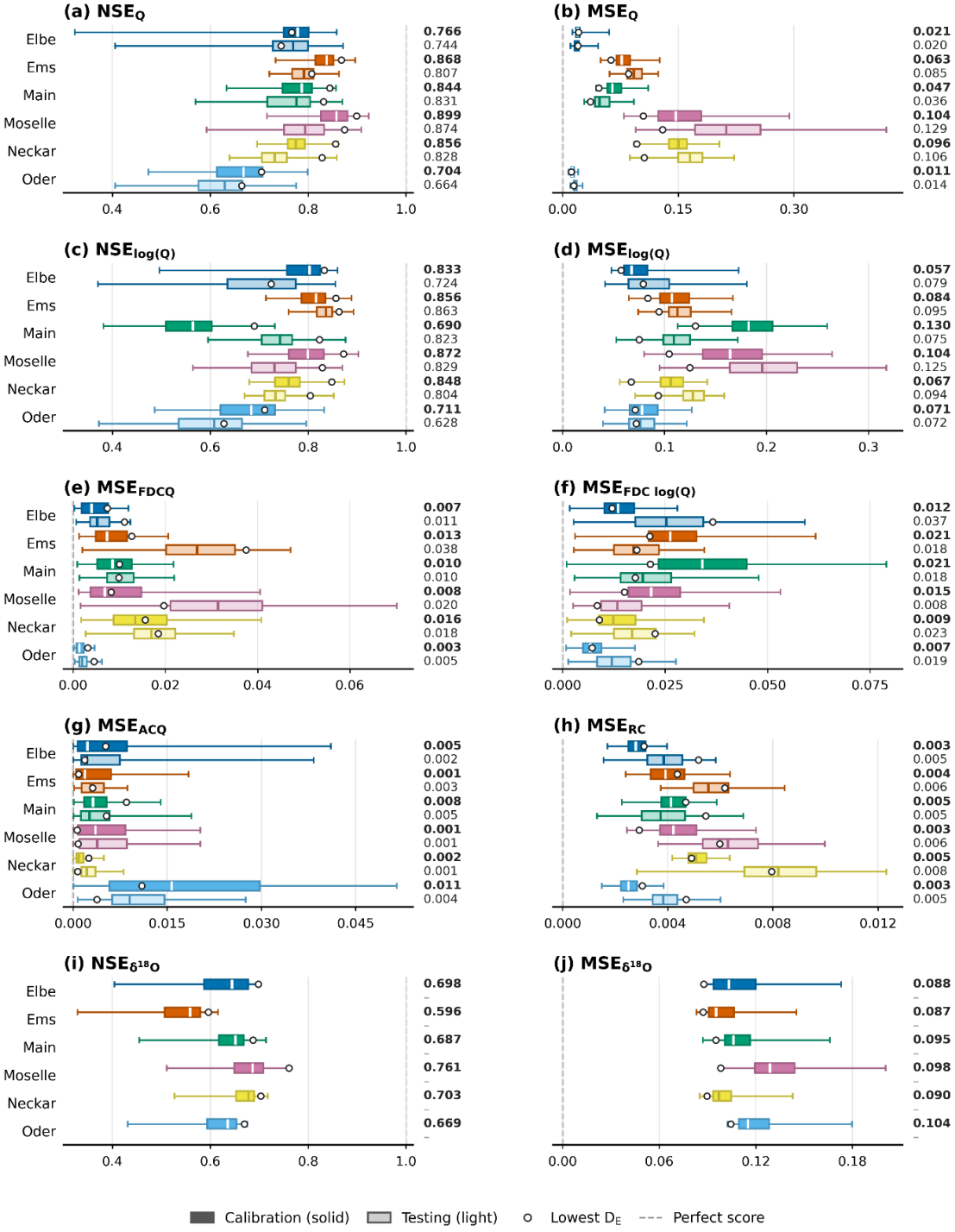

Figure 5 Performance measures of the Pareto-optimal parameter sets for the six catchments during calibration (solid boxes) and testing (light boxes), expressed as NSE and MSE for discharge (Q), log-transformed discharge [log(Q)], the flow-duration curve (FDC), autocorrelation (AC), seasonal runoff coefficient (RC), and $\delta^{18}O$. Dots and numbers indicate the performance of the parameter set with the lowest (D_E). Dashed lines denote perfect performance (NSE = 1; MSE = 0).

https://doi.org/10.5194/egusphere-2026-6810
Preprint. Discussion started: 25 November 2026
© Author(s) 2026. CC BY 4.0 License.

5.2 TTDs and water-age fractions of high-, intermediate- and low flows

The modelled streamflow magnitudes within each flow condition spanned from 0.55 to 9.32 mm d^{-1} for high flows ($Q_m > Q_{m,10}$), from 0.16 to 1.93 mm d^{-1} for intermediate flows ($Q_{m,90} \leq Q_m \leq Q_{m,10}$), and from 0.03 to 0.61 mm d^{-1} for low flows ($Q_m < Q_{m,90}$). The basin-specific discharge thresholds used to define the flow quantiles are listed in Supplementary Material Tab. S8 e.g., $Q_{m,10}$: 0.55–1.94 mm d^{-1} and $Q_{m,90}$: 0.16–0.61 mm d^{-1} across the six study basins. High-flow events predominantly occurred from late autumn to early spring, with 73.5 % of all high-flows concentrated between November and March. Conversely, 81.8 % of low flows were concentrated between July and November, while intermediate flows were more evenly distributed throughout the year. Across the six basins, median cumulative TTDs, estimated based on daily TTDs over the 2001–2020 period, showed a consistent pattern: high flows were associated with younger water-ages than intermediate flows, whereas low flows were dominated by older water-ages (Fig. 6 d-f). When considering water-age fractions at the opposite ends of the TTDs, median f_{90} contribution was greatest during high flows, ranging from 0.30 to 0.52 across basins, decreasing to 0.20–0.34 during intermediate flows and to 0.06–0.20 during low flows (Fig. 6 a-c). Conversely, median f_{older} contribution accounted for a substantial fraction under all three flow conditions and was greatest during low flows, ranging from 0.34–0.51 for high flows, from 0.55–0.72 for intermediate flows and from 0.74–0.88 for low flows across basins (Fig. 6 g-i). Across basins, median young-water fractions increased from low to high flows by a factor of 2.4–3.0: f_{10} increased from 0.03 to 0.09 (3.0-fold increase), f_{30} from 0.09 to 0.22 (2.4-fold increase), and f_{90} from 0.15 to 0.44 (2.9-fold increase).

When focusing on individual basins, median f_{90} generally increased from low through intermediate to high streamflow conditions (Fig. 6). However, the sensitivity of water-age composition to streamflow conditions differed among basins. The Neckar basin showed particularly high sensitivity, with median f_{90} increasing from 0.06 under low flows to 0.20 under intermediate flows and 0.51 under high flows. Similarly, f_{90} increased strongly in the Moselle (f_{90} = 0.17–0.52), Ems (f_{90} = 0.12–0.48) and Main (f_{90} = 0.11–0.41). In contrast, the Oder and Elbe were more stable throughout low, intermediate and high flow conditions, with f_{90} changing from 0.20 to 0.23 and 0.32 in the Oder and from 0.19 to 0.30 in the Elbe. All water-age fractions across high, intermediate and low flow conditions for individual basins are provided in Fig. S5 in the supplementary material.

https://doi.org/10.5194/egusphere-2026-6810
Preprint. Discussion started: 25 November 2026
© Author(s) 2026. CC BY 4.0 License.

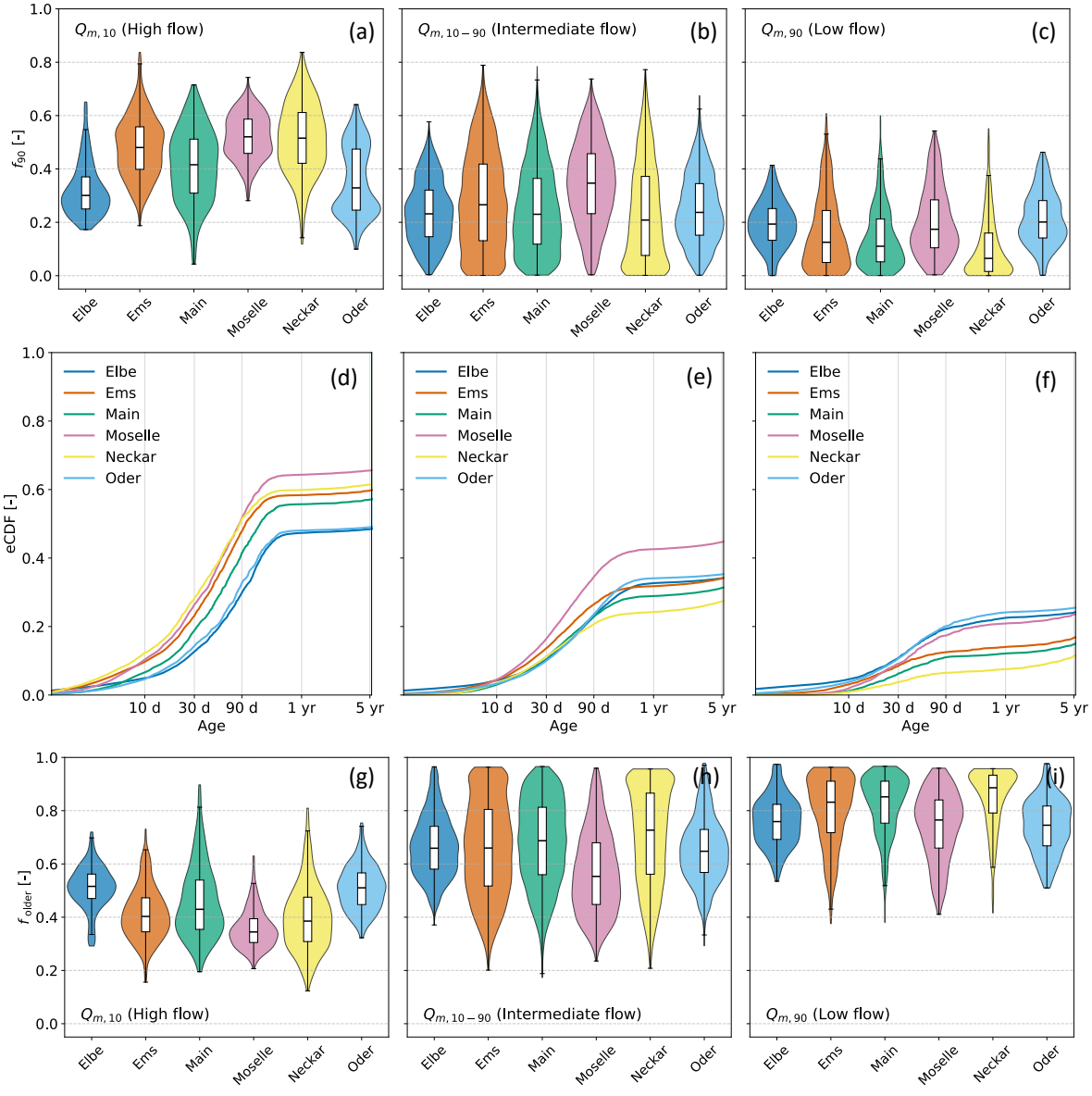

Figure 6: Top row fraction of water younger than 90 days (f_{90}) of all basins during (a) high flows, (b) intermediate flows and (c) low flows. Middle row (d-f): Median TTDs estimated for the Elbe, Ems, Main, Moselle, Neckar, and Oder watersheds under (d) high flow conditions ($Q_m > Q_{m,10}$), (e) intermediate flow conditions ($Q_{m,90} \leq Q_m \leq Q_{m,10}$) and (f) low flow conditions ($Q_m < Q_{m,90}$). Bottom row: fraction of water older than 5 years (f_{older}) of all basins during (g) high flows, (h) intermediate flows and (i) low flows.

https://doi.org/10.5194/egusphere-2026-6810
Preprint. Discussion started: 25 November 2026
© Author(s) 2026. CC BY 4.0 License.

5.3 Intra-annual variability of TTDs and water-age fractions

Seasonal TTDs suggest that median fractions of younger water (i.e., f_{10}, f_{30}, f_{90}) were overall larger in summer and autumn than in winter and spring across basins (Fig. 7). This seasonal pattern was most pronounced at high and intermediate flows but also distinguishable under low-flow conditions. Summer consistently exhibited larger f_{30} across high (0.42), intermediate (0.24), and low flows (0.09), than winter with 0.21, 0.08, and 0.03, respectively. Summer and winter f_{30} distributions showed non-overlapping IQRs at high and intermediate flows and only minimal IQR overlap at low flows. This seasonal contrast is illustrated by the selected winter and summer high flow events in Fig. 8. Consistent with differences seen in the median TTDs, the events show greater relative contributions of f_{10} and f_{30}, during summer high flows than during winter high flows.

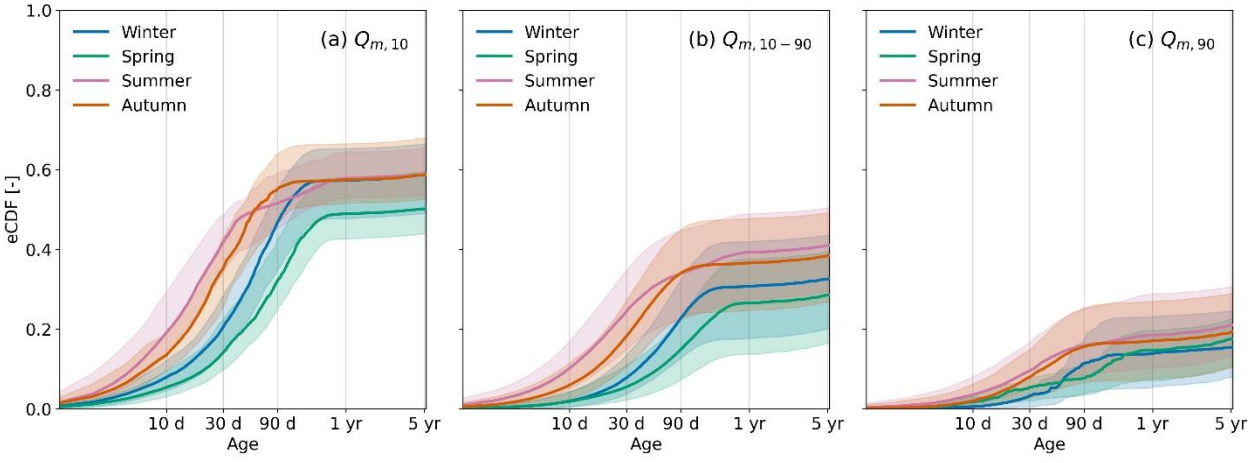

Figure 7: Seasonal TTDs for (a) high ($Q_m > Q_{m,10}$), (b) intermediate ($Q_{m,90} \leq Q_m \leq Q_{m,10}$) and (c) low flows ($Q_m < Q_{m,90}$). The figure shows the median TTDs (solid lines) and interquartile range (shaded areas) separated by season. The data was aggregated from all six basins.

Intra-annual variability in the f_{90} water-age fraction differed markedly among basins and flow states (Fig. 9 a). Summer and autumn median f_{90} were 9–57 % and 21–49 % larger than the annual median at high flows, respectively. The highest summer median f_{90} = 0.73 occurred in the Ems, whereas the highest autumn f_{90} = 0.64 occurred in the Neckar. In contrast, spring median f_{90} was 12–26 % lower than the annual median. At intermediate flows, summer and autumn median f_{90} were up to 54 % and 51 % higher than the annual median, respectively, whereas spring values were 26–47 % lower. Winter median f_{90} showed no consistent deviation from the annual median across basins. Seasonal differences were small at low flows: summer and autumn median f_{90} differed from the annual median by +4 % and +1 %, respectively. Winter and spring f_{90} medians were not assessed because low-flow events were rare or absent during these seasons. Seasonal shifts between high- and low-flow f_{90} were most pronounced in the Neckar and Main basins, whereas they were weaker in the Oder and Elbe basins (Fig. 9 a). Most notably, in the latter two basins, autumn low-flow f_{90} was comparable to spring high-flow f_{90}. Across all basins, the largest high-flow f_{90} occurred between July and November, while peak low-flow f_{90} was restricted mainly to August–October. Conversely, f_{older} was larger in winter than in summer at intermediate (0.67 vs. 0.59) and low flows (0.84 vs. 0.79)

https://doi.org/10.5194/egusphere-2026-6810
Preprint. Discussion started: 25 November 2026
© Author(s) 2026. CC BY 4.0 License.

but was identical at high flows (0.41) across basins. Complementary, the intra-annual variability of f_{older} can be obtained from Fig. 9 b for all six basins.

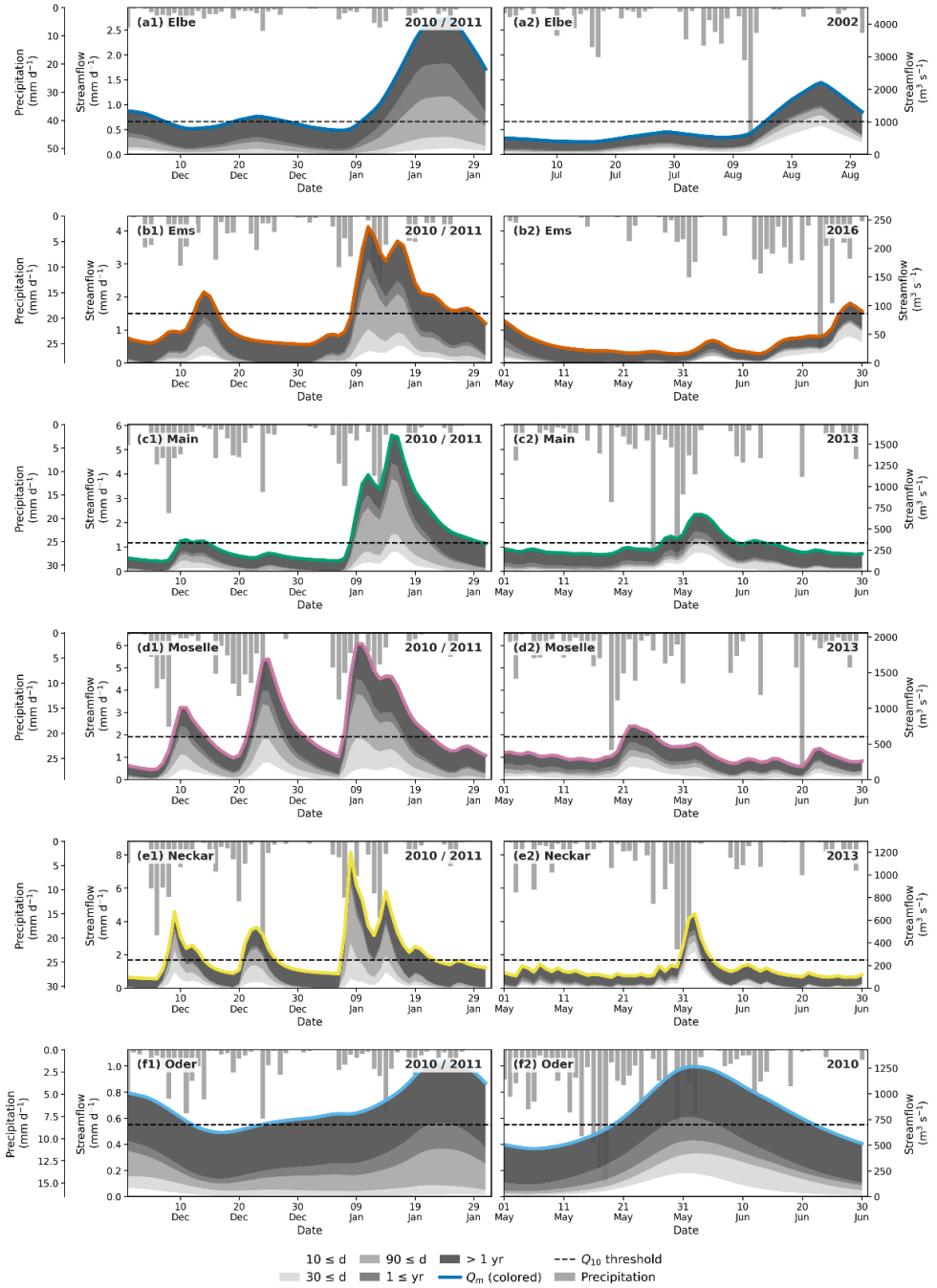

490 **Figure 8:** Exemplary summer (1) and winter (2) high flow events for Elbe (a), Ems (b), Main (c), Moselle (d), Neckar (e), and Oder (f). The hydrograph was partitioned into water-age fractions, shaded from light grey (younger) to dark grey (older); Modelled streamflow Q_m in color. Precipitation is shown in grey as downward pointing bars at the top of each subplot. The same figure, but with a y-axis ranging from 0 to 1, showing the normalized fractions of water ages at each time step, can be found in Fig. S6 of the Supplementary Material.

https://doi.org/10.5194/egusphere-2026-6810
Preprint. Discussion started: 25 November 2026
© Author(s) 2026. CC BY 4.0 License.

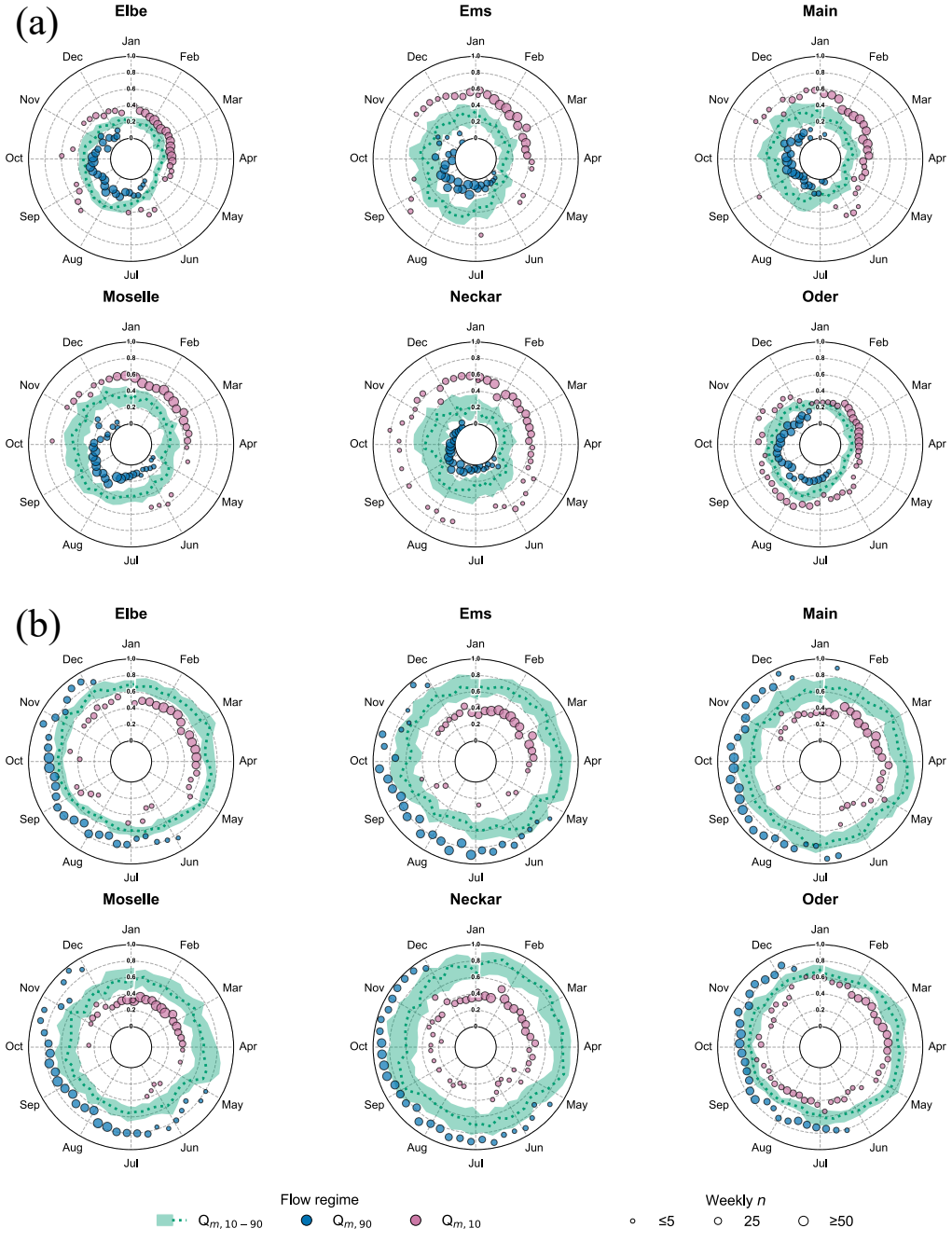

Figure 9: Intra-annul variability of (a) f_{90} and (b) f_{older} for Elbe, Ems, Main, Moselle, Neckar, and Oder under intermediate ($Q_{m,90} \leq Q_m \leq Q_{m,10}$), low ($Q_m < Q_{m,90}$) and high ($Q_m > Q_{m,10}$) flow conditions across the study period Oct. 2001 – Dec. 2020. Each polar plot shows the annual cycle, the radial distance from the center indicates (a) f_{90} and (b) f_{older}, the angle represents the time of year. Both, f_{90} and f_{older} are shown as weekly medians. For high- and low-flow conditions, weekly medians are represented by circular markers, with marker size proportional to the number of flow events (n) contributing to each median. For intermediate-flow conditions, weekly medians are shown using equally sized markers, and shaded areas indicate the interquartile range (IQR). This representation avoids overlap with the low- and high-flow f_{90} and f_{older} water-age fractions, as intermediate flows comprise 80 % of flow conditions by its definition.

https://doi.org/10.5194/egusphere-2026-6810
Preprint. Discussion started: 25 November 2026
© Author(s) 2026. CC BY 4.0 License.

5.4 Influential factors and f_{90} sensitivity

Water-age fractions showed considerable variation across all flow conditions, which could not be explained by a single variable. Among tested variables (see section 4.6), we identified Q_m and $SPEI_{30}$ as the most influential factors, consistently exhibiting the strongest Spearman rank correlation coefficients (r_s) and showing consistent patterns with water-age fractions across basins (Tab. 5). Younger-water fractions (f_{10}, f_{30}, and f_{90}) were positively correlated with Q_m and $SPEI_{30}$, whereas f_{older} was negatively correlated. Correlations with Q_m generally increased from f_{10} to f_{90} and were strongest in Neckar and Mosel, particularly for f_{90} (r_s = 0.57 in both basins), compared with weaker correlations in Elbe (r_s = 0.28) and Oder (r_s = 0.26). In contrast, f_{older} showed consistently strong negative correlations with Q_m across all basins (r_s = −0.53 to −0.67). For the younger-water fractions, correlations with $SPEI_{30}$ were generally stronger than those with Q_m. The strongest positive $SPEI_{30}$ correlations occurred for f_{30} and f_{90} in Main, Mosel, Elbe, and Oder, with r_s values ranging from 0.61 to 0.68. The strongest negative $SPEI_{30}$ correlation for f_{older} occurred in Oder (r_s = −0.72), while the weakest occurred in Neckar (r_s = −0.40). When aggregating normalized discharge ($Q_m/Q_{m,mean}$), $SPEI_{30}$, and water-age fractions across all basins into 30 equally sized discharge-quantile classes, the water-age fractions changed systematically along the discharge and $SPEI_{30}$ gradients (Fig. 10). Younger-water fractions were lowest under low-flow conditions associated with dry antecedent conditions and increased towards high-flow, wet conditions, whereas f_{older} decreased. From the lowest to the highest quantile class, median $SPEI_{30}$ increased from −1.3 to 1.2 and normalized discharge increased from 0.15 mm d^{-1} to 3.35 mm d^{-1}. Over the same range, f_{10}, f_{30}, and f_{90} increased by 0.10, 0.19, and 0.39, respectively, whereas f_{older} decreased by 0.47. Theil-Sen slopes indicated that water-age fractions were less sensitive to changes in discharge in Elbe and Oder than in the other basins, particularly for the younger-water fractions (Fig. 10; Tab 5). This contrast was most pronounced for f_{90}, which increased by 0.17 per mm d^{-1} in the Neckar basin, compared with 0.08 per mm d^{-1} in the Oder basin and 0.07 per mm d^{-1} in the Elbe basin. Thus, the discharge sensitivity of f_{90} in the Neckar basin was 113 % higher than in the Oder basin and 143 % higher than in the Elbe basin. Neckar also showed the steepest discharge-related increase in f_{30} and the strongest decline in f_{older} (−0.20 per mm d^{-1}), further emphasizing its high discharge sensitivity. For f_{90}, Main, Mosel, and Ems showed slopes of 0.11–0.13 per mm d^{-1}, indicating discharge sensitivities between the high sensitivity in Neckar and the lower sensitivities in Elbe and Oder. In contrast, Sen slopes for $SPEI_{30}$ varied modestly among the six basins (Tab. 5). For f_{90}, slopes ranged from 0.08 to 0.10 per $SPEI_{30}$ unit, while those for f_{older} ranged from −0.08 to −0.11 per $SPEI_{30}$ unit. The complete Spearman-rank correlation matrices for all tested variables and basins can be found in Supplementary Material Fig. S7.

https://doi.org/10.5194/egusphere-2026-6810
Preprint. Discussion started: 25 November 2026
© Author(s) 2026. CC BY 4.0 License.

Table 2: Spearman rank correlations coefficients (r_s) and Theil-Sen slopes (β) between water-age fractions (f_{10}, f_{30}, f_{90}, f_{older}) and normalized discharge ($Q_m/Q_{m,mean}$) and $SPEI_{30}$ for all six river basins. * indicates a statistically significant Spearman correlation ($p < 0.05$). † indicates that the 95 % confidence interval of the Theil–Sen slope excludes zero. Values shown as >0.00 are non-zero values smaller than 0.005 in absolute terms.

	Basin	Elbe		Ems		Main		Moselle		Neckar		Oder	
Variable	Statistic	r_s	β	r_s	β	r_s	β	r_s	β	r_s	β	r_s	β
$Q_m/Q_{m,mean}$	f_{10}	0.03*	>0.00†	0.20*	0.02†	0.22*	0.01†	0.32*	0.02†	0.38*	0.03†	0.10*	0.01†
	f_{30}	0.08*	0.01†	0.24*	0.05†	0.23*	0.04†	0.36*	0.05†	0.44*	0.09†	0.13*	0.03†
	f_{90}	0.28*	0.07†	0.46*	0.13†	0.42*	0.11†	0.57*	0.11†	0.57*	0.17†	0.26*	0.08†
	f_{older}	−0.55*	−0.13†	−0.54*	−0.15†	−0.56*	−0.17†	−0.67*	−0.14†	−0.61*	−0.20†	−0.53*	−0.15†
$SPEI_{30}$	f_{10}	0.55*	0.02†	0.40*	0.03†	0.46*	0.02†	0.42*	0.03†	0.36*	0.02†	0.55*	0.02†
	f_{30}	0.61*	0.05†	0.56*	0.08†	0.68*	0.07†	0.68*	0.09†	0.50*	0.07†	0.60*	0.05†
	f_{90}	0.67*	0.08†	0.48*	0.10†	0.62*	0.10†	0.57*	0.10†	0.43*	0.08†	0.68*	0.09†
	f_{older}	−0.65*	−0.08†	−0.45*	−0.10†	−0.58*	−0.11†	−0.51*	−0.10†	−0.40*	−0.08†	−0.72*	−0.10†

https://doi.org/10.5194/egusphere-2026-6810
Preprint. Discussion started: 25 November 2026
© Author(s) 2026. CC BY 4.0 License.

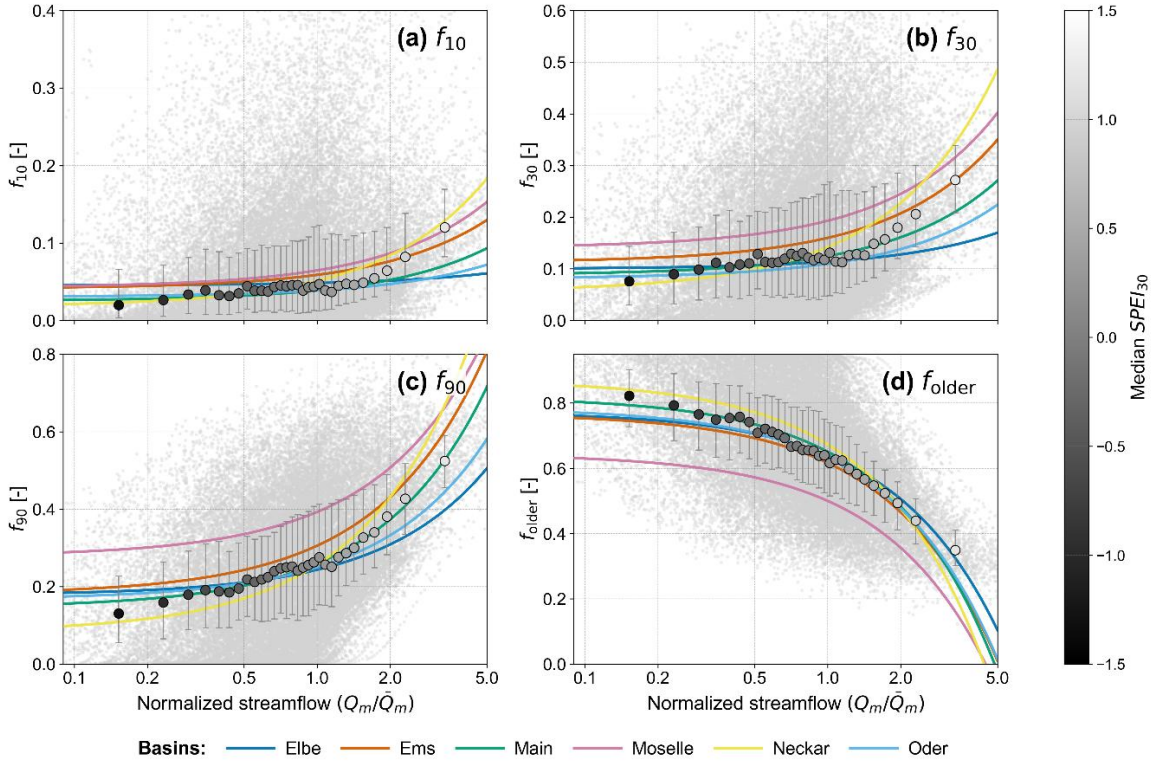

Figure 10: Normalized streamflow ($Q_m/Q_{m,mean}$) and $SPEI_{30}$ against water-age fractions (a) f_{10}, (b) f_{30}, (c) f_{90}, and (d) f_{older} across all six basins. The data from all basins is aggregated and subsequently grouped into 30 equally sized streamflow-quantile classes. The markers represent the median water-age fraction, and the error bars show the interquartile range of each class. The marker color indicates the median $SPEI_{30}$, where black represents dry antecedent conditions and light gray is wet antecedent conditions of the previous 30 days. Colored lines show Theil-Sen linear fits for each of the Elbe, Ems, Main, Moselle, Neckar, and Oder basins. Single data points are shown as grey dots in the background.

6. Discussion

6.1 Substantial young water contributions – even in large basins

Contrary to the common intuition that discharge in large river basins may be dominated by older water, we found substantial contributions of younger water across all six basins. The long-term cross basin mean f_{90} was 0.27, indicating that, on average, more than one quarter of streamflow was younger than 90 days. Median younger water fractions across basins increased from 0.04 (IQR: 0.01–0.1) for f_{10} to 0.12 (IQR: 0.05–0.23) for f_{30} and 0.25 (IQR: 0.14 – 0.39) for f_{90}. Notably, these young water contributions are substantial compared with cross catchment mean f_{yw} values reported in previous studies of small to meso-scale catchments. In comparison, von Freyberg et al. (2018) reported f_{yw} values ranging from 0.07 to 0.49, with a median f_{yw} of 0.16, across 22 Swiss catchments. Floriancic et al. (2024) calculated both f_{yw} and the fraction of new water (f_{new}), defined as water younger than one month, for 32 Alpine catchments. Their study complemented the Swiss catchments investigated by von Freyberg et al. (2018) with river data from Austria. They found a mean f_{yw} of 0.14, ranging

https://doi.org/10.5194/egusphere-2026-6810
Preprint. Discussion started: 25 November 2026
© Author(s) 2026. CC BY 4.0 License.

from 0.10 to 0.17, and a mean f_{new} of 0.07, ranging from 0.03 to 0.09. Lutz et al. (2018) estimated f_{yw} across 24 contrasting sub catchments within the Bode catchment in Germany, with catchment areas ranging from 0.11 to 200 km², and reported a mean f_{yw} of 0.11, with values ranging from 0.01 to 0.27. In the Hubbard Brook catchment, Benettin et al. (2017) found that the fraction of streamflow younger than two months remained at or above 0.35 during a two-month high-flow period. Globally, our mean f_{90} across basins (0.27) closely matches the global average young-streamflow fraction of 0.26 reported by Jasechko et al. (2016) for 254 rivers worldwide. Together with previous large-scale studies (Wang et al., 2023; Stockinger and Stumpp, 2024), our results show that young water is a substantial component of streamflow even in large river basins. Our f_{90} estimates show strong agreement with previously published f_{yw} for the same basins despite the methodological differences (Stockinger and Stumpp, 2024). We compared the long-term mean f_{90}, derived from daily estimates over 2001–2016, with the time-varying $f_{yw\text{-}vari}$ reported by Stockinger and Stumpp (2024) for the same basins and period. A key distinction lies in the methodology: f_{90} (fraction ≤90 days) represents the mean of daily fractions calculated for the full-time series, whereas $f_{yw\text{-}vari}$ (fraction <~3 months), reported in Stockinger and Stumpp (2024), is the mean of 172 estimates from a seasonal sine-wave method applied over one-year moving windows. Despite these differences, the basin mean values were closely aligned ($f_{yw\text{-}vari}$: 0.21–0.39; f_{90}: 0.24–0.34), with a mean absolute difference of only ~0.04 and identical cross-basin averages of 0.27. However, the SD of our daily-derived f_{90} (mean SD = 0.16; range 0.11–0.19) was predictably higher than that of the annually-windowed $f_{yw\text{-}vari}$ (mean SD ≈ 0.10; range 0.06–0.21). This discrepancy is an expected artifact of temporal aggregation, a phenomenon demonstrated by Wang et al. (2025), who showed that the variability of f_{yw} substantially contracts when moving from daily to longer time scales. To confirm this effect in our own data, we recalculated the f_{90} statistics from annual-mean values instead of daily ones. This procedure, which mimics the temporal scale of the $f_{yw\text{-}vari}$ estimates, reduced the mean SD of f_{90} across basins to 0.02, while the overall mean f_{90} remained unchanged at 0.27. Furthermore, our results for the Neckar basin are consistent with those of Wang et al. (2023), who used a similar tracer-aided model calibrated against $\delta^{18}O$ and streamflow. Our long-term mean f_{90} of 0.25±0.19 for the Neckar falls within their reported f_{yw} range of 0.23–0.29 (representing the 5th/95th percentile across all Pareto-optimal parameter sets).

6.2 Hydrological controls on the discharge–age relationship

Our results show that stream-water age was jointly influenced by flow state and season. Across the studied basins, f_{90} increased from a median of 0.14 during low flows (IQR: 0.08–0.23) to 0.25 during intermediate flows (IQR: 0.14–0.37) and 0.42 during high flows (IQR: 0.34–0.51). This progressive increase indicates that higher discharge was associated with stronger contributions of younger-water fractions, consistent with previous studies showing that wet conditions and high flows activate fast near-surface, shallow subsurface, riparian, and hillslope flow paths that preferentially deliver younger water to streams (e.g., Soulsby et al., 2015; Wilusz et al., 2017; von Freyberg et al., 2018). Similar discharge sensitivity of young-water fractions has been reported across Swiss catchments, where high-flow periods were interpreted to contain larger fractions of young water travelling through fast flow paths, while low flows were mainly sustained by older groundwater (e.g., von Freyberg et al., 2018). The intermediate-flow condition represented a clear transition between low- and high-flow

https://doi.org/10.5194/egusphere-2026-6810
Preprint. Discussion started: 25 November 2026
© Author(s) 2026. CC BY 4.0 License.

conditions, suggesting that stream-water age changed gradually rather than shifting abruptly between old and young end members. Despite the increase in young water with discharge, high flows were not composed solely of recent precipitation. Water older than 5 years remained a substantial component even during high flows, with a median contribution of 0.43 (IQR: 0.35–0.52), and became increasingly dominant during intermediate flows, with a median of 0.65 (IQR: 0.54–0.77), and low flows, with a median of 0.80 (IQR: 0.70–0.88). This persistence of old water is consistent with the "old-water paradox" (Bishop, 1991; Kirchner, 2003) and also agrees with event peaks where new precipitation water is mixed with water previously stored in the catchment, rather than consisting solely of event water (e.g., McDonnell, 1990) emphasizing the conceptual difference between celerity and velocity (Rodríguez-Iturbe and Valdés, 1979; Gupta et al., 1980).

Seasonality modulated the discharge-age relationship, showing that flow state alone does not determine TTDs. Although high flows generally mobilized a larger proportion of young water, the relationship between discharge and younger-water contributions varied markedly among seasons. Stream water was generally younger in autumn and summer than in winter and spring, with the strongest seasonal contrasts occurring during high flows. This pattern was evident for both the f_{90} and f_{30} water-age fractions. Across basins, median high-flow f_{90} values were 0.55 (IQR: 0.46–0.64) in autumn and 0.51 (IQR: 0.45–0.59) in summer, compared with 0.47 (IQR: 0.35–0.55) in winter and 0.32 (IQR: 0.25–0.42) in spring. The contrast was even more pronounced in the f_{30} median values, which were 0.36 (IQR: 0.26–0.43) in autumn and 0.42 (IQR: 0.34–0.48) in summer and 0.21 (IQR: 0.14–0.29) in winter and 0.14 (IQR: 0.10–0.22) in spring. This suggests that, although summer and autumn high-flow events may be less frequent, they activated rapid near-surface or shallow subsurface pathways effectively. This seasonal pattern is broadly consistent with Floriancic et al. (2024), who showed that monthly new-water and young-water fractions in Alpine rivers are higher in summer than in winter; with their summer new-water fraction comparable to the f_{30} metric used in this study. In our case, the higher summer–autumn young-water fractions likely reflect event-driven activation of fast pathways, whereas lower winter–spring values suggest stronger contributions from older storage. Intermediate flows further show that discharge alone did not fully determine stream-water age. Median f_{90} values during intermediate flows were highest in autumn and summer, at 0.34 (IQR: 0.22–0.45) and 0.33 (IQR: 0.22–0.44), respectively, and lower in autumn and spring, at 0.23 (IQR: 0.12–0.32) and 0.15 (IQR: 0.07–0.23). This indicates that similar flow states can be associated with different young-water fractions depending on season and catchment state. A robust seasonal comparison of low flows was not possible because low-flow conditions occurred almost exclusively in summer and autumn. Nevertheless, their low f_{90} values and high fractions of water older than 5 years indicate that low-flow discharge was dominated by older storage. Overall, our results agree with previous evidence that young- or new-water fractions generally increase under wetter and higher-flow conditions (e.g., Soulsby et al., 2015; Wilusz et al., 2017; von Freyberg et al., 2018), but they also show that this discharge dependence is seasonally modulated (Wang et al., 2025).

6.4 Variability in water-age fractions and f_{90} sensitives

Despite the general tendency for younger water (f_{10}, f_{30}, f_{90}) fractions to be larger under wetter and higher-flow conditions, and to be lower under dryer and low flow conditions, substantial variability remained across flow conditions and seasons.

https://doi.org/10.5194/egusphere-2026-6810
Preprint. Discussion started: 25 November 2026
© Author(s) 2026. CC BY 4.0 License.

For example, 20% of intermediate flows and 5% of low flows had f_{90} fractions higher than the median f_{90} of high flows across basins, indicating that intermediate and even low flows can contain considerable proportions of f_{90}. Similarly, only part of the largest 10 % of f_{90} values coincided with the largest 10 % of discharge within each flow condition. Intermediate flows showed the widest spread, with f_{90} ranging from 0.02 to 0.72, suggesting that this condition integrates a particularly broad range of hydrological and transport states. The Spearman rank correlation analysis identified Q_m and $SPEI_{30}$ explaining part, but not all, of this variability. Most other tested hydroclimatic variables showed only weak to moderate correlations with water-age fractions. Low flows were mostly associated with dry conditions, intermediate flows with near-normal conditions, and high flows with wet conditions. However, the large scatter indicates that neither discharge nor $SPEI_{30}$ alone is sufficient to predict water-age composition across flow states. In particular, intermediate flows can occur during event rise, event recession, seasonal wetting, seasonal drying, or groundwater-supported baseflow recovery, each of which may be associated with different water-age mixtures (e.g., Rodriguez et al., 2018). Therefore, the wide range of f_{90} values observed in intermediate flows reflects not only variability in discharge magnitude or $SPEI_{30}$, but also differences in antecedent conditions, event timing, storage state, and the contribution from different flow-paths. This interpretation is consistent with evidence that discharge selection preferences are temporally variable and that subsurface mixing schemes shift through time, with preferential selection of younger water during wet periods and a gradual shift toward older water during drying, dry, and wetting periods (e.g., Harman, 2015; van der Velde et al., 2015; Rodriguez et al., 2018; Hrachowitz et al., 2021). While our analysis provides insight into the general behaviour of large basins, a more detailed understanding of variability within individual basins requires dedicated basin-specific studies. Future work could use event-based approaches (e.g., Tang and Carey, 2017) to explicitly link precipitation dynamics, runoff responses, and event-specific transit-time distributions rather than relying solely on fixed flow- condition thresholds.

Among the six basins, the discharge sensitivity of f_{90} varied markedly, ranging from relatively buffered responses to pronounced shifts between low- and high-flow conditions. Accordingly, differences in median f_{90} between high- and low-flow conditions were consistent with these basin-specific sensitivities. Median high-flow f_{90} was 8.0 and 3.0 times as high as low-flow f_{90} in the Neckar and Moselle, respectively, but only 1.5 and 1.6 times as high in the Elbe and Oder. Correspondingly, Theil-Sen slopes were 2.1 times as high in the Neckar as in the Oder and 1.3 times as high in the Moselle as in the Elbe. In contrast, sensitivity of f_{90} to $SPEI_{30}$ varied little among basins, indicating a more uniform influence of antecedent wetness. Overall, all basins shifted rapidly between lower and higher f_{90} fractions, although the magnitude differed considerably. Attributing differences in f_{90} sensitivity to specific basins characteristics was challenging because all basins exhibited substantial internal heterogeneity in landscape characteristics and hydrological processes. As a conceptual framework, von Freyberg et al. (2018) interpreted low discharge sensitivity as indicating relatively stable contributions from fast and slow flow paths, whereas high sensitivity reflected event-driven shifts in the dominant flow paths. However, our outlet-scale analysis could not resolve these internal dynamics in depth given the large scales. We therefore hypothesized that the comparatively low f_{90} sensitivity of the Elbe and Oder partly resulted from the attenuation of high-flow signals along their longer flow paths and across their flatter terrain. The river-flow paths of Elbe and Oder were 2,046 and 1,207 km long,

https://doi.org/10.5194/egusphere-2026-6810
Preprint. Discussion started: 25 November 2026
© Author(s) 2026. CC BY 4.0 License.

respectively, which was 2.8 to 6.8 times the lengths of those in the Neckar (301 km) and Moselle (429 km). Moreover, areas with slopes ≥10° accounted for only 5.2 % of the Elbe basin and 2.3 % of the Oder basin, compared with 14.8% of the Neckar basin and 13.6 % of the Moselle basin. Although flow-path heterogeneity is implicitly captured in the integrated response at the catchment outlet, our analysis represented it only through the aggregate contributions of fast flow (Q_f) and slow flow (Q_s) to Q_m. Further resolving the specific hydrological processes and flow pathways represented by Q_f and Q_s, including their spatial organization and activation under different hydrological conditions, would require more detailed, spatially distributed hydrological analyses.

6.5 Limitations and Uncertainty

The model structure used here was a simple representation of basin functioning rather than a direct reproduction of the real complexity of the system. As with any hydrological model, the results are conditional on the chosen perceptual model, structural assumptions, parameterization, and available observations (Beven, 2006). Although greater structural complexity and finer spatial resolution could in principle represent additional processes and spatial heterogeneity, such complexity and resolution are only useful if they can be constrained and evaluated with available observations; otherwise, they may increase uncertainty without necessarily improving realism or predictive value (e.g., Beven and Binley, 1992; Jakeman and Hornberger, 1993; Beven, 2006). Consequently, the present results should be understood as an evaluation of whether the implemented conceptual model and the uniform SAS-based mixing assumption are consistent with the available data, rather than as evidence for a unique description of the real basin system. In particular, equifinality remains a key limitation, because alternative choices of model structures, process parametrizations and parameter sets, may yield similarly acceptable simulations when observations are sparse to discriminate further among them (e.g., Beven and Freer, 2001; Beven, 2006), as recently also demonstrated by Türk et al. (2026a) for the choice of mixing assumptions and thus SAS function shapes. Flow conditions were defined using the modelled discharge, because TTDs and water-age fractions are derived from modelled flows and must be consistent with the model's water balance. The discrepancies between simulated and observed discharge were more pronounced at low and high flows than at intermediate flows, with ΔQ10 ranging from −0.3 % to −16.3 % and ΔQ90 from −0.9 % to −9.1 %, which may partly reflect increased observational uncertainty under extreme flow conditions. For example, low-flow estimates can be affected by limited gauge resolution; this may be relevant for the Frankfurt Osthafen station used for the Main catchment, where discharge values at the lower end of the range are reported with relatively coarse resolution. However, the measurement uncertainty of streamflow increases at both low- and high-flows as rating curves often require extrapolation beyond the range of direct discharge measurements used to establish the rating curve, and hydraulic controls may become unstable (McMillan et al., 2012; Kiang et al., 2018).

Comparison with MODIS snow-cover data suggests that modelled snow cover has no systematic bias, as underestimation and overestimation errors were nearly balanced with 4.3 % and 4.1 %, respectively. While snow-cover overestimation may delay meltwater release and bias TTDs towards older ages, underestimation may have the opposite effect. Given the close balance between both snow-cover error types, their net influence on the overall median water-age fractions is expected to be

https://doi.org/10.5194/egusphere-2026-6810
Preprint. Discussion started: 25 November 2026
© Author(s) 2026. CC BY 4.0 License.

minor. Future work could incorporate snow-cover observations as an additional calibration constraint to improve the representation of snow dynamics in the model.

7. Summary and conclusion

This study showed that all six large Central European basins had substantial younger-water contributions (median f_{90} = 0.23–0.35) and that their TTDs and water-age fractions varied systematically with flow condition and season. At these large spatial scales, transitions toward younger streamflow under high-flow conditions were pronounced, indicating shifts in the dominant water sources and flow pathways. Across basins, median f_{90} during high flows was 1.7 times as high as during intermediate flows and 2.8 times as high during low flows. However, the relationship between discharge and water age was seasonally modulated and more pronounced during high and intermediate flow conditions. During high flows, median f_{30} was higher in summer (0.42) and autumn (0.36) than in winter (0.21) and spring (0.14), while median f_{90} was higher in autumn (0.51) than in spring (0.32). Besides this seasonal modulation, the streamflow-age sensitivities differed among basins ranging from relatively stable water-age compositions across flow conditions in some basins to stronger shifts between younger and older water contributions in others i.e., median f_{90} during high flows was ranging from 1.5 to 8 times as high as under low flow conditions. In conclusion, our study challenges the common intuition that streamflow in large river basins is dominated primarily by older water. Instead, all six basins showed substantial contributions of younger water that were comparable to or even higher than those reported for small- to meso-scale catchments. As climate change is expected to alter hydrological conditions and, in many regions, increase the frequency and intensity of both high and low flows, the contributions of young versus older water to streamflow may become increasingly important in large river basins. Across the six basins, younger-water contributions generally increased under high-flow conditions, whereas low flows were characterized by a greater dominance of older water. However, the magnitude of these water-age shifts varied strongly among basins and seasons, and the hydroclimatic variables considered in this study explained only part of the observed water-age variability, leaving important controls to be resolved in future research.

https://doi.org/10.5194/egusphere-2026-6810
Preprint. Discussion started: 25 November 2026
© Author(s) 2026. CC BY 4.0 License.

Code and data availability

The equations used in the model are described in supplementary material and this manuscript. Hydroclimatic data used in this study is available from: E-OBS (Cornes et al., 2018), GRDC (grdc.bafg.de), MODIS/Terra Snow Cover (Hall and Riggs, 2021). Stable Isotope data is available from: Piso.Ai (Nelson et al., 2021), the German Isotope Network (GIN; isotopes-GIN.de), and from the corresponding author upon request.

Author contributions

KK, MH and CS designed the study. KK carried out the analysis and drafted the manuscript. All authors contributed to the overall idea and participated in the discussion and writing of the manuscript.

Competing interests

Some authors are members of the editorial board of the HESS journal.

Acknowledgements

This work was funded by the Austrian Science Fund (FWF—Österreichischer Wissenschaftsfonds) [Grant 10. 55776/DOC216]. The work of Karl Knaebel was additionally supported by the Doctoral School “Human River Systems in the 21st Century (HR21)” of the BOKU University, Vienna. ChatGPT (GPT-4 and GPT-5.6) and Gemini 3 Pro, accessed through Academic AI – BOKU instance, were used to provide language suggestions and assist with Python/Matplotlib code for the figures during manuscript preparation. Open Access funding is provided by BOKU University.

Financial support

This research has been supported by the Austrian Science Fund (R/VF) grant no.10. 55776/DOC216.

https://doi.org/10.5194/egusphere-2026-6810
Preprint. Discussion started: 25 November 2026
© Author(s) 2026. CC BY 4.0 License.

References

Adams, J.: climate_indices, an open source Python library providing reference implementations of commonly used climate indices, https://github.com/monocongo/climate_indices, 2025.

Arsenault, R., Brissette, F., and Martel, J.-L.: The hazards of split-sample validation in hydrological model calibration, Journal of Hydrology, 566, 346–362, doi:10.1016/j.jhydrol.2018.09.027, 2018.

Benettin, P., Bailey, S. W., Campbell, J. L., Green, M. B., Rinaldo, A., Likens, G. E., McGuire, K. J., and Botter, G.: Linking water age and solute dynamics in streamflow at the H ubbard B rook E xperimental F orest, NH USA, Water Resour. Res., 51, 9256–9272, doi:10.1002/2015WR017552, 2015a.

Benettin, P., Kirchner, J. W., Rinaldo, A., and Botter, G.: Modeling chloride transport using travel time distributions at Plynlimon, Wales, Water Resour. Res., 51, 3259–3276, doi:10.1002/2014WR016600, 2015b.

Benettin, P., Rodriguez, N. B., Sprenger, M., Kim, M., Klaus, J., Harman, C. J., van der Velde, Y., Hrachowitz, M., Botter, G., McGuire, K. J., Kirchner, J. W., Rinaldo, A., and McDonnell, J. J.: Transit Time Estimation in Catchments: Recent Developments and Future Directions, Water Resources Research, 58, e2022WR033096, doi:10.1029/2022WR033096, 2022.

Benettin, P., Soulsby, C., Birkel, C., Tetzlaff, D., Botter, G., and Rinaldo, A.: Using SAS functions and high-resolution isotope data to unravel travel time distributions in headwater catchments, Water Resources Research, 53, 1864–1878, doi:10.1002/2016WR020117, 2017.

Bergström, S.: The HBV Model: Its Structure and Applications,Swedish Meteorological and Hydrological Institute (SMHI): Hydrology, 35 pp., 1992.

Beven, K.: A manifesto for the equifinality thesis, Journal of Hydrology, 320, 18–36, doi:10.1016/j.jhydrol.2005.07.007, 2006.

Beven, K. and Binley, A.: The future of distributed models: Model calibration and uncertainty prediction, Hydrological Processes, 6, 279–298, doi:10.1002/hyp.3360060305, 1992.

Beven, K. and Freer, J.: Equifinality, data assimilation, and uncertainty estimation in mechanistic modelling of complex environmental systems using the GLUE methodology, Journal of Hydrology, 249, 11–29, doi:10.1016/S0022-1694(01)00421-8, 2001.

Birkel, C. and Soulsby, C.: Advancing tracer-aided rainfall–runoff modelling: a review of progress, problems and unrealised potential, Hydrological Processes, 29, 5227–5240, doi:10.1002/hyp.10594, 2015.

Birkel, C., Soulsby, C., and Tetzlaff, D.: Modelling catchment-scale water storage dynamics: reconciling dynamic storage with tracer-inferred passive storage, Hydrological Processes, 25, 3924–3936, doi:10.1002/hyp.8201, 2011.

Bishop, K. H.: Episodic Increases in Stream Acidity, Catchment Flow Pathways and Hydrograph Separation, 1991.

Botter, G., Bertuzzo, E., and Rinaldo, A.: Catchment residence and travel time distributions: The master equation, Geophys. Res. Lett., 38, n/a-n/a, doi:10.1029/2011GL047666, 2011.

https://doi.org/10.5194/egusphere-2026-6810
Preprint. Discussion started: 25 November 2026
© Author(s) 2026. CC BY 4.0 License.



Cartwright, I. and Morgenstern, U.: Transit times from rainfall to baseflow in headwater catchments estimated using tritium: the Ovens River, Australia, Hydrol. Earth Syst. Sci., 19, 3771–3785, doi:10.5194/hess-19-3771-2015, 2015.

Cornes, R. C., van der Schrier, G., van den Besselaar, E. J. M., and Jones, P. D.: An Ensemble Version of the E-OBS Temperature and Precipitation Data Sets, J. Geophys. Res., 123, 9391–9409, doi:10.1029/2017JD028200, 2018.

DeWalle, D. R., Edwards, P. J., Swistock, B. R., Aravena, R., and Drimmie, R. J.: Seasonal isotope hydrology of three Appalachian forest catchments, Hydrological Processes, 11, 1895–1906, doi:10.1002/(SICI)1099-1085(199712)11:15<1895:AID-HYP538>3.0.CO;2-#, 1997.

do Nascimento, T. V. M., Rudlang, J., Höge, M., van der Ent, R., Chappon, M., Seibert, J., Hrachowitz, M., and Fenicia, F.: EStreams: An integrated dataset and catalogue of streamflow, hydro-climatic and landscape variables for Europe, Sci Data, 11, 879, doi:10.1038/s41597-024-03706-1, 2024.

EEA: CORINE Land Cover (CLC) 2018, Version 2020_20u1, Copernicus Land Monitoring Service, European Environment Agency, Copenhagen, Denmark, https://land.copernicus.eu/pan-european/corine-land-cover/clc2018, 2020.

Euser, T., Hrachowitz, M., Winsemius, H. C., and Savenije, H. H.: The effect of forcing and landscape distribution on performance and consistency of model structures, Hydrological Processes, 29, 3727–3743, doi:10.1002/hyp.10445, 2015.

Fenicia, F., Wrede, S., Kavetski, D., Pfister, L., Hoffmann, L., Savenije, H. H. G., and McDonnell, J. J.: Assessing the impact of mixing assumptions on the estimation of streamwater mean residence time, Hydrological Processes, 24, 1730–1741, doi:10.1002/hyp.7595, 2010.

Floriancic, M. G., Stockinger, M. P., Kirchner, J. W., and Stumpp, C.: Monthly new water fractions and their relationships with climate and catchment properties across Alpine rivers, Hydrol. Earth Syst. Sci., 28, 3675–3694, doi:10.5194/hess-28-3675-2024, 2024.

Fovet, O., Ruiz, L., Hrachowitz, M., Faucheux, M., and Gascuel-Odoux, C.: Hydrological hysteresis and its value for assessing process consistency in catchment conceptual models, Hydrol. Earth Syst. Sci., 19, 105–123, doi:10.5194/hess-19-105-2015, 2015.

Gallart, F., Freyberg, J. von, Valiente, M., Kirchner, J. W., Llorens, P., and Latron, J.: Technical note: An improved discharge sensitivity metric for young water fractions, Hydrol. Earth Syst. Sci., 24, 1101–1107, doi:10.5194/hess-24-1101-2020, 2020.

Gao, H., Ding, Y., Zhao, Q., Hrachowitz, M., and Savenije, H. H.: The importance of aspect for modelling the hydrological response in a glacier catchment in Central Asia, Hydrological Processes, 31, 2842–2859, doi:10.1002/hyp.11224, 2017.

Girons Lopez, M., Vis, M. J. P., Jenicek, M., Griessinger, N., and Seibert, J.: Assessing the degree of detail of temperature-based snow routines for runoff modelling in mountainous areas in central Europe, Hydrol. Earth Syst. Sci., 24, 4441–4461, doi:10.5194/hess-24-4441-2020, 2020.

GTOPO30: Global 30 Arc-Second Elevation (GTOPO30).

https://doi.org/10.5194/egusphere-2026-6810
Preprint. Discussion started: 25 November 2026
© Author(s) 2026. CC BY 4.0 License.

Gupta, V. K., Waymire, E., and Wang, C. T.: A representation of an instantaneous unit hydrograph from geomorphology, Water Resour. Res., 16, 855–862, doi:10.1029/WR016i005p00855, 1980.

Hachgenei, N., Nord, G., Spadini, L., Ginot, P., Voiron, C., and Duwig, C.: Transit time tracing using wetness-adaptive StorAge Selection functions—application to a Mediterranean catchment, Journal of Hydrology, 638, 131267, doi:10.1016/j.jhydrol.2024.131267, 2024.

Hakala, K., Addor, N., Teutschbein, C., Vis, M., Dakhlaoui, H., and Seibert, J.: Hydrological Modeling of Climate Change Impacts, in: Encyclopedia of Water, John Wiley & Sons, Ltd, 1–20, 2019.

Hall, D. and Riggs, G.: MODIS/Terra Snow Cover 8-Day L3 Global 500m SIN Grid, Version 61, 2021.

Harman, C. J.: Time-variable transit time distributions and transport: Theory and application to storage-dependent transport of chloride in a watershed, Water Resour. Res., 51, 1–30, doi:10.1002/2014WR015707, 2015.

Hrachowitz, M., Benettin, P., van Breukelen, B. M., Fovet, O., Howden, N. J., Ruiz, L., van der Velde, Y., and Wade, A. J.: Transit times—the link between hydrology and water quality at the catchment scale, Wiley Interdisciplinary Reviews: Water, 3, 629–657, doi:10.1002/wat2.1155, 2016.

Hrachowitz, M., Fovet, O., Ruiz, L., and Savenije, H. H. G.: Transit time distributions, legacy contamination and variability in biogeochemical 1/f α scaling: how are hydrological response dynamics linked to water quality at the catchment scale?, Hydrological Processes, 29, 5241–5256, doi:10.1002/hyp.10546, 2015.

Hrachowitz, M., Savenije, H., Bogaard, T. A., Tetzlaff, D., and Soulsby, C.: What can flux tracking teach us about water age distribution patterns and their temporal dynamics?, Hydrol. Earth Syst. Sci., 17, 533–564, doi:10.5194/hess-17-533-2013, 2013.

Hrachowitz, M., Stockinger, M., Coenders-Gerrits, M., van der Ent, R., Bogena, H., Lücke, A., and Stumpp, C.: Reduction of vegetation-accessible water storage capacity after deforestation affects catchment travel time distributions and increases young water fractions in a headwater catchment, Hydrol. Earth Syst. Sci., 25, 4887–4915, doi:10.5194/hess-25-4887-2021, 2021.

Intergovernmental Panel on Climate Change (IPCC): Weather and Climate Extreme Events in a Changing Climate, in: Climate Change 2021 – The Physical Science Basis: Working Group I Contribution to the Sixth Assessment Report of the Intergovernmental Panel on Climate Change, Cambridge University Press, 1513–1766, 2023.

Jakeman, A. J. and Hornberger, G. M.: How much complexity is warranted in a rainfall-runoff model?, Water Resour. Res., 29, 2637–2649, doi:10.1029/93WR00877, 1993.

Jasechko, S., Kirchner, J. W., Welker, J. M., and McDonnell, J. J.: Substantial proportion of global streamflow less than three months old, Nature Geosci, 9, 126–129, doi:10.1038/ngeo2636, 2016.

Kiang, J. E., Gazoorian, C., McMillan, H., Coxon, G., Le Coz, J., Westerberg, I. K., Belleville, A., Sevrez, D., Sikorska, A. E., Petersen-Øverleir, A., Reitan, T., Freer, J., Renard, B., Mansanarez, V., and Mason, R.: A Comparison of Methods for Streamflow Uncertainty Estimation, Water Resour. Res., 54, 7149–7176, doi:10.1029/2018WR022708, 2018.

https://doi.org/10.5194/egusphere-2026-6810
Preprint. Discussion started: 25 November 2026
© Author(s) 2026. CC BY 4.0 License.

Kirchner, J. W.: A double paradox in catchment hydrology and geochemistry, Hydrological Processes, 17, 871–874, doi:10.1002/hyp.5108, 2003.

Kirchner, J. W.: Aggregation in environmental systems – Part 1: Seasonal tracer cycles quantify young water fractions, but not mean transit times, in spatially heterogeneous catchments, Hydrol. Earth Syst. Sci., 20, 279–297, doi:10.5194/hess-20-279-2016, 2016a.

Kirchner, J. W.: Aggregation in environmental systems – Part 2: Catchment mean transit times and young water fractions under hydrologic nonstationarity, Hydrol. Earth Syst. Sci., 20, 299–328, doi:10.5194/hess-20-299-2016, 2016b.

Klaus, J. and McDonnell, J. J.: Hydrograph separation using stable isotopes: Review and evaluation, Journal of Hydrology, 505, 47–64, doi:10.1016/j.jhydrol.2013.09.006, 2013.

Koeniger, P., Stumpp, C., and Schmidt, A.: Stable isotope patterns of German rivers with aspects on scales, continuity and network status, Isotopes in Environmental and Health Studies, 58, 363–379, doi:10.1080/10256016.2022.2127702, 2022.

Lehner, B. and Grill, G.: Global river hydrography and network routing: baseline data and new approaches to study the world's large river systems, Hydrological Processes, 27, 2171–2186, doi:10.1002/hyp.9740, 2013.

Lutz, S. R., Krieg, R., Müller, C., Zink, M., Knöller, K., Samaniego, L., and Merz, R.: Spatial Patterns of Water Age: Using Young Water Fractions to Improve the Characterization of Transit Times in Contrasting Catchments, Water Resour. Res., 54, 4767–4784, doi:10.1029/2017WR022216, 2018.

Małoszewski, P., Rauert, W., Stichler, W., and Herrmann, A.: Application of flow models in an alpine catchment area using tritium and deuterium data, Journal of Hydrology, 66, 319–330, doi:10.1016/0022-1694(83)90193-2, 1983.

Małoszewski, P. and Zuber, A.: Determining the turnover time of groundwater systems with the aid of environmental tracers, Journal of Hydrology, 57, 207–231, doi:10.1016/0022-1694(82)90147-0, 1982.

McDonnell, J. J.: A Rationale for Old Water Discharge Through Macropores in a Steep, Humid Catchment, Water Resour. Res., 26, 2821–2832, doi:10.1029/WR026i011p02821, 1990.

McDonnell, J. J., McGuire, K., Aggarwal, P., Beven, K. J., Biondi, D., Destouni, G., Dunn, S., James, A., Kirchner, J., Kraft, P., Lyon, S., Maloszewski, P., Newman, B., Pfister, L., Rinaldo, A., Rodhe, A., Sayama, T., Seibert, J., Solomon, K., Soulsby, C., Stewart, M., Tetzlaff, D., Tobin, C., Troch, P., Weiler, M., Western, A., Wörman, A., and Wrede, S.: How old is streamwater? Open questions in catchment transit time conceptualization, modelling and analysis, Hydrological Processes, 24, 1745–1754, doi:10.1002/hyp.7796, 2010.

McGuire, K. J. and McDonnell, J. J.: A review and evaluation of catchment transit time modeling, Journal of Hydrology, 330, 543–563, doi:10.1016/j.jhydrol.2006.04.020, 2006.

McMillan, H., Krueger, T., and Freer, J.: Benchmarking observational uncertainties for hydrology: rainfall, river discharge and water quality, Hydrological Processes, 26, 4078–4111, doi:10.1002/hyp.9384, 2012.

https://doi.org/10.5194/egusphere-2026-6810
Preprint. Discussion started: 25 November 2026
© Author(s) 2026. CC BY 4.0 License.

Morgenstern, U., Stewart, M. K., and Stenger, R.: Dating of streamwater using tritium in a post nuclear bomb pulse world: continuous variation of mean transit time with streamflow, Hydrol. Earth Syst. Sci., 14, 2289–2301, doi:10.5194/hess-14-2289-2010, 2010.

Mostbauer, K., Kaitna, R., Prenner, D., and Hrachowitz, M.: The temporally varying roles of rainfall, snowmelt and soil moisture for debris flow initiation in a snow-dominated system, Hydrol. Earth Syst. Sci., 22, 3493–3513, doi:10.5194/hess-22-3493-2018, 2018.

Nash, J. E. and Sutcliffe, J. V.: River flow forecasting through conceptual models part I — A discussion of principles, Journal of Hydrology, 10, 282–290, doi:10.1016/0022-1694(70)90255-6, 1970.

Nelson, D. B., Basler, D., and Kahmen, A.: Precipitation isotope time series predictions from machine learning applied in Europe, Proceedings of the National Academy of Sciences of the United States of America, 118, e2024107118, doi:10.1073/pnas.2024107118, 2021.

Nijzink, R., Hutton, C., Pechlivanidis, I., Capell, R., Arheimer, B., Freer, J., Han, D., Wagener, T., McGuire, K., Savenije, H., and Hrachowitz, M.: The evolution of root-zone moisture capacities after deforestation: a step towards hydrological predictions under change?, Hydrol. Earth Syst. Sci., 20, 4775–4799, doi:10.5194/hess-20-4775-2016, 2016.

Parajka, J. and Blöschl, G.: The value of MODIS snow cover data in validating and calibrating conceptual hydrologic models, Journal of Hydrology, 358, 240–258, doi:10.1016/j.jhydrol.2008.06.006, 2008.

Pearce, A. J., Stewart, M. K., and Sklash, M. G.: Storm Runoff Generation in Humid Headwater Catchments: 1. Where Does the Water Come From?, Water Resour. Res., 22, 1263–1272, doi:10.1029/WR022i008p01263, 1986.

Prenner, D., Kaitna, R., Mostbauer, K., and Hrachowitz, M.: The Value of Using Multiple Hydrometeorological Variables to Predict Temporal Debris Flow Susceptibility in an Alpine Environment, Water Resour. Res., 54, 6822–6843, doi:10.1029/2018WR022985, 2018.

Reckerth, A., Stichler, W., Schmidt, A., and Stumpp, C.: Long-term data set analysis of stable isotopic composition in German rivers, Journal of Hydrology, 552, 718–731, doi:10.1016/j.jhydrol.2017.07.022, 2017.

Rinaldo, A., Benettin, P., Harman, C. J., Hrachowitz, M., McGuire, K. J., van der Velde, Y., Bertuzzo, E., and Botter, G.: Storage selection functions: A coherent framework for quantifying how catchments store and release water and solutes, Water Resources Research, 51, 4840–4847, doi:10.1002/2015WR017273, 2015.

Rodriguez, N. B., McGuire, K. J., and Klaus, J.: Time-Varying Storage–Water Age Relationships in a Catchment With a Mediterranean Climate, Water Resour. Res., 54, 3988–4008, doi:10.1029/2017WR021964, 2018.

Rodriguez, N. B., Pfister, L., Zehe, E., and Klaus, J.: A comparison of catchment travel times and storage deduced from deuterium and tritium tracers using StorAge Selection functions, Hydrol. Earth Syst. Sci., 25, 401–428, doi:10.5194/hess-25-401-2021, 2021.

Rodríguez-Iturbe, I. and Valdés, J. B.: The geomorphologic structure of hydrologic response, Water Resour. Res., 15, 1409–1420, doi:10.1029/WR015i006p01409, 1979.

https://doi.org/10.5194/egusphere-2026-6810
Preprint. Discussion started: 25 November 2026
© Author(s) 2026. CC BY 4.0 License.

Sawicz, K. A., Kelleher, C., Wagener, T., Troch, P., Sivapalan, M., and Carrillo, G.: Characterizing hydrologic change through catchment classification, Hydrol. Earth Syst. Sci., 18, 273–285, doi:10.5194/hess-18-273-2014, 2014.

Shen, H., Tolson, B. A., and Mai, J.: Time to Update the Split-Sample Approach in Hydrological Model Calibration, Water Resour. Res., 58, e2021WR031523, doi:10.1029/2021WR031523, 2022.

Sklash, M. G., Beven, K. J., GILMAN, K., and DARLING, W. G.: ISOTOPE STUDIES OF PIPEFLOW AT PLYNLIMON, WALES, UK, Hydrol. Process., 10, 921–944, doi:10.1002/(SICI)1099-1085(199607)10:7<921:AID-HYP347>3.0.CO;2-B, 1996.

Sklash, M. G., Stewart, M. K., and Pearce, A. J.: Storm Runoff Generation in Humid Headwater Catchments: 2. A Case Study of Hillslope and Low-Order Stream Response, Water Resour. Res., 22, 1273–1282, doi:10.1029/WR022i008p01273, 1986.

Soulsby, C., Birkel, C., Geris, J., Dick, J., Tunaley, C., and Tetzlaff, D.: Stream water age distributions controlled by storage dynamics and nonlinear hydrologic connectivity: Modeling with high-resolution isotope data, Water Resour. Res., 51, 7759–7776, doi:10.1002/2015WR017888, 2015.

Sprenger, M., Stumpp, C., Weiler, M., Aeschbach, W., Allen, S. T., Benettin, P., Dubbert, M., Hartmann, A., Hrachowitz, M., Kirchner, J. W., McDonnell, J. J., Orlowski, N., Penna, D., Pfahl, S., Rinderer, M., Rodriguez, N., Schmidt, M., and Werner, C.: The Demographics of Water: A Review of Water Ages in the Critical Zone, Reviews of Geophysics, 57, 800–834, doi:10.1029/2018RG000633, 2019.

Stadnyk, T. A. and Holmes, T. L.: Large scale hydrologic and tracer aided modelling: A review, Journal of Hydrology, 618, 129177, doi:10.1016/j.jhydrol.2023.129177, 2023.

Stockinger, M. P. and Stumpp, C.: Lessons learned from the spatiotemporal analysis of long-term and time-variable young water fractions of large central European river basins, Hydrological Processes, 38, e15038, doi:10.1002/hyp.15038, 2024.

Storn, R. and Price, K.: Differential Evolution – A Simple and Efficient Heuristic for global Optimization over Continuous Spaces, Journal of Global Optimization, 11, 341–359, doi:10.1023/A:1008202821328, 1997.

Tang, W. and Carey, S. K.: Hyd R un: A MATLAB toolbox for rainfall–runoff analysis, Hydrological Processes, 31, 2670–2682, doi:10.1002/hyp.11185, 2017.

Tong, R., Parajka, J., Széles, B., Greimeister-Pfeil, I., Vreugdenhil, M., Komma, J., Valent, P., and Blöschl, G.: The value of satellite soil moisture and snow cover data for the transfer of hydrological model parameters to ungauged sites, Hydrol. Earth Syst. Sci., 26, 1779–1799, doi:10.5194/hess-26-1779-2022, 2022.

Türk, H., Stumpp, C., Hrachowitz, M., Schulz, K., Strauss, P., Blöschl, G., and Stockinger, M.: Soil moisture and precipitation intensity jointly control the transit time distribution of quick flow in a flashy headwater catchment, Hydrol. Earth Syst. Sci., 29, 3935–3956, doi:10.5194/hess-29-3935-2025, 2025.

https://doi.org/10.5194/egusphere-2026-6810
Preprint. Discussion started: 25 November 2026
© Author(s) 2026. CC BY 4.0 License.



Türk, H., Stumpp, C., Hrachowitz, M., Strauss, P., Blöschl, G., and Stockinger, M.: Catchment transit time variability with different SAS function parameterizations for the unsaturated zone and groundwater, Hydrol. Earth Syst. Sci., 30, 1053–1076, doi:10.5194/hess-30-1053-2026, 2026a.

Türk, H., Stumpp, C., Stockinger, M., and Benettin, P.: Tracking Event-Scale Precipitation Partitioning Reveals Comparable Roles of Event Characteristics and Seasonality in Shaping Precipitation Fate in a Forested Landscape, Hydrological Processes, 40, e70466, doi:10.1002/hyp.70466, 2026b.

van der Velde, Y., Heidbüchel, I., Lyon, S. W., Nyberg, L., Rodhe, A., Bishop, K., and Troch, P. A.: Consequences of mixing assumptions for time-variable travel time distributions, Hydrological Processes, 29, 3460–3474, doi:10.1002/hyp.10372, 2015.

van der Velde, Y., Torfs, P. J. J. F., van der Zee, S. E. A. T. M., and Uijlenhoet, R.: Quantifying catchment-scale mixing and its effect on time-varying travel time distributions, Water Resour. Res., 48, doi:10.1029/2011WR011310, 2012.

Vicente-Serrano, S. M., Beguería, S., and López-Moreno, J. I.: A Multiscalar Drought Index Sensitive to Global Warming: The Standardized Precipitation Evapotranspiration Index, Journal of Climate, 23, 1696–1718, doi:10.1175/2009JCLI2909.1, 2010.

von Freyberg, J., Allen, S. T., Seeger, S., Weiler, M., and Kirchner, J. W.: Sensitivity of young water fractions to hydro-climatic forcing and landscape properties across 22 Swiss catchments, Hydrol. Earth Syst. Sci., 22, 3841–3861, doi:10.5194/hess-22-3841-2018, 2018.

Vořechovský, M.: Hierarchical Refinement of Latin Hypercube Samples, Computer aided Civil Eng, 30, 394–411, doi:10.1111/mice.12088, 2015.

Vremec, M., Collenteur, R. A., and Birk, S.: PyEt v1.3.1: a Python package for the estimation of potential evapotranspiration, Geosci. Model Dev., 17, 7083–7103, doi:10.5194/gmd-17-7083-2024, 2024.

Wang, S., Hrachowitz, M., Schoups, G., and Störiko, A.: Multi-decadal stability of water ages and tracer transport in a temperate-humid river basin, Environ. Res. Lett., doi:10.1088/1748-9326/ada8c1, 2025.

Wang, S., Hrachowitz, M., Schoups, G., and Stumpp, C.: Stable water isotopes and tritium tracers tell the same tale: no evidence for underestimation of catchment transit times inferred by stable isotopes in StorAge Selection (SAS)-function models, Hydrol. Earth Syst. Sci., 27, 3083–3114, doi:10.5194/hess-27-3083-2023, 2023.

Wilusz, D. C., Harman, C. J., and Ball, W. P.: Sensitivity of Catchment Transit Times to Rainfall Variability Under Present and Future Climates, Water Resour. Res., 53, 10231–10256, doi:10.1002/2017WR020894, 2017.

Yang, J., Heidbüchel, I., Musolff, A., Xie, Y., Lu, C., and Fleckenstein, J. H.: Using nitrate as a tracer to constrain age selection preferences in catchments with strong seasonality, Journal of Hydrology, 603, 126889, doi:10.1016/j.jhydrol.2021.126889, 2021.

Zuber, A.: On the interpretation of tracer data in variable flow systems, Journal of Hydrology, 86, 45–57, doi:10.1016/0022-1694(86)90005-3, 1986.